AN ANALYSIS ON THE APPLICATION OF ALGEBRAIC GEOMETRY IN INITIAL ORBIT DETERMINATION PROBLEMS

A Dissertation
Presented to
The Academic Faculty

By

Michela Mancini

In Partial Fulfillment
of the Requirements for the Degree
Master of Science in the
School of Aerospace Engineering
Department of Aerospace Engineering

Georgia Institute of Technology
&
Sapienza University of Rome

December 2022

AN ANALYSIS ON THE APPLICATION OF ALGEBRAIC GEOMETRY IN INITIAL ORBIT DETERMINATION PROBLEMS

Thesis committee:

Dr. John A. Christian
School of Aerospace Engineering
Georgia Institute of Technology

Dr. Brian C. Gunter
School of Aerospace Engineering
Georgia Institute of Technology

Dr. Anton Leykin
School of Mathematics
Georgia Institute of Technology

Date approved: 11/16/2022

ACKNOWLEDGMENTS

I would like to thank the members of the committee for their help in the preparation of this work. I am grateful to my advisor, Dr. Christian, for introducing me to the world of astrodynamics seen through the lenses of geometry. His enthusiasm and his expertise have been inspiring throughout this year. I want to thank Dr. Leykin, whose competence and whose notes on algebraic geometry have been the first fundamental step for the comprehension of the mathematical instruments used in this work. Last but not least, I want to thank Dr. Gunter, whose critical eye was a precious source of food for thoughts.

A special thank goes to Dr. Duff, who has spent time and energy guiding me inside the world of Macaulay2. Without his help, nothing of this would have been possible in the same time span.

I am indebted to my dearest friends in Italy, who stood by me despite kilometers away, and to my friends and colleagues here, for the friendly and happy environment they created. Thanks to who made me feel my house here like my home.

I cannot express the gratitude I feel towards my parents and my brothers. You have always been the cornerstones I needed, and you gave me the mental serenity to make this step.

The author gratefully acknowledges support for this research from the Air Force Office of Scientific Research (AFOSR) under the Space University Research Initiative (SURI) through grant FA95502210092 (PI: Dr. John Crassidis from SUNY-Buffalo; managed by Dr. Stacie Williams and Dr. Fariba Fahroo from AFOSR).

TABLE OF CONTENTS

LIST OF TABLES

LIST OF FIGURES

LIST OF ACRONYMS

GEO Geosynchronous Equatorial Orbit

IOD Initial Orbit Determination

LEO Low Earth Orbit

LOS line of sight

OD Orbit Determination

POD Precise Orbit Determination

QMM QUEST Measurement Model

SUMMARY

Initial Orbit Determination (IOD) is a classical problem in astrodynamics. The space around Earth is crowded by a great many objects whose orbits are unknown, and the number of space debris is constantly increasing because of break-up events and collisions. Reconstructing the orbit of a body from observations allows us to create catalogs that are used to avoid collisions and program missions for debris removal. Also, comparing the observations of celestial bodies with predictions of their positions made based on our knowledge of the universe has been in the past, and is still today, one of the most effective means to make improvements in our cosmological model. In this work, a purely geometric solution to the angles-only IOD problem is analyzed, and its performance under various scenarios of observations is tested. The problem formulation is based on a re-parameterization of the orbit as a disk quadric, and relating the observations to the unknowns leads to a polynomial system that can be solved using tools from numerical algebraic geometry. This method is time-free and does not require any type of initialization. This makes it unaffected by the problems related to the estimate of the time-of-flight, that usually affects the accuracy of the solution. A similar approach may be used to analyze the performance of the solver when streaks are used, together with lines of sight, as inputs to the problem. Streaks on digital images form, together with the camera location, planes that are tangent to the orbit. This produces two different types of constraints, that can be written as polynomial equations. The accuracy and the robustness of the solver are decreased by the presence of streaks, but they remain a valid input when diversity in the observed directions guarantees the departure from the singular configuration of almost coplanar observations.

CHAPTER 1
INTRODUCTION AND MOTIVATION

1.1 Initial Orbit Determination: definition and motivation

Orbit Determination (OD) is the process through which the trajectory of a body in space is recovered. It is one of the most ancient problems in astrodynamics and has attracted, over the centuries, the interest of the most famous mathematicians and astronomers. This problem is as vast as it is complex, and can be stated using many different formulations. The complete OD process requires many elements, like a sufficiently accurate dynamical model, a collection of observations of the orbiting object, and algorithms and filters to analyze these data at increasing levels of depth. We can divide the whole OD process as happening into two main steps. Assume an object is observed for the first time in space, and no information is available about its orbit. The first action is to obtain an initial guess of what the object's trajectory is. This is the task of Initial Orbit Determination (IOD) methods. Afterward, Precise Orbit Determination (POD) methods are used to optimally estimate the orbit through filters that exploit the most in-depth knowledge of the specific dynamical environment that rules the motion of the body considered. However, the vast majority of these POD algorithms needs to be initialized, and the first initial guess is, by definition, given by IOD solutions.

This work will focus on a solution to the IOD problem that is strictly geometric, and for this reason we will primarily concentrate on IOD characterization. In fact, IOD processes can vary depending on the assumptions made at the basis of the problem and on the type of measurements available. However, all the IOD methods are united by the absence of any kind of *a priori* information about the orbit. We can then state the problem of Initial Orbit Determination (IOD) as the process of determining the trajectory followed by a body when

it is seen for the first time, and no a priori information is available about it.

Classical IOD methods are based on the assumption that the orbit followed by the body is Keplerian. These are the most basic types of IOD since they do not make any assumption on the dynamical model except for the presence of a massive body that creates a gravitational attraction as described by Newton's universal law of gravitation. The categorization based on the type of measurements used gives rise to the definition of *angles-only* IOD methods as those based on line of sight (LOS) observations, where the object is sighted, for example, by means of a telescope or a camera. This type of observation is "angles-only" because the only information that it provides is a direction in space, a line that intersects the orbit, and is usually described in terms of a pair of angles - right ascension and declination from a specific observing site. Another big class of IOD methods is populated by those based on the knowledge of the range information: the whole position vector of the body is known at certain points along the orbit. Other variants exploit the knowledge of the velocity vector of the satellite at certain positions [1] [2] or make use of streaks on digital images [3]. In this work, a solution to the classic angles-only IOD problem will be studied. In the first part, only LOS measurements will be considered, while in the second part they will be combined with streak observations.

However, one may wonder what are the motivations behind the study of OD. In the past, when even the orbits of the planets of our own solar system were unknown, a method that allowed us to recover the details about their motion was desirable for obvious reasons. In the XVII century the Ptolemaic model was still widespread and the equations ruling the dynamics of the celestial bodies were far from being understood. The exactness of the predictions of the positions of the celestial bodies made by the astronomers using Newton's gravitational law, reflecting Kepler's intuitions, represented a turning point, proving that the heliocentric model was a more accurate description of the solar system than the geocentric architecture that many people were still trying to defend. Nowadays, the orbits of the celestial bodies of our solar system are well known, and their position in the future can be

predicted with great precision even taking into account different types of perturbations. But there is an infinitely high number of celestial bodies whose orbits are unknown: planets, moons, stars, comets, that may have never been spotted until now. Also, our knowledge of the universe and its physics is limited. In the currently accepted cosmological model, dark matter has been introduced to explain phenomena otherwise unexplainable using the law of gravitation applied to the visible matter [4]. This dark matter contributes to determining the orbit of the bodies in space, and this consideration makes now clear the role that orbit determination can have in the study of the dynamics and the physics of our universe: comparing the observations made with the predictions, as already done in the past, is a means that allows us to discover discrepancies between our cosmological model and the reality. This is part of a process that can be summarized as trying to ”match the *fitter's universe* with the *real universe*”[5][6]. Coming back closer to the Earth, we can identify another undeniable use for fast, precise OD. The space around the Earth is crowded by a great many objects whose orbits are unknown, and that represent a danger for every other satellites in orbit around the Earth or spacecrafts in transit directed to farther destinations [7]. Further, the number of space debris is increasing because of breakup events and collisions, and an as vast as possible catalog of the objects residing in space would help in preventing collisions and planning missions for the removal of debris. This passes through the determination of the orbits of the sighted objects.

Clearly, the level of accuracy in the estimation of the orbit needed to fulfill the scopes described above is not given by an IOD algorithm. However, we have already seen how it is a fundamental step before a more accurate description can be made using POD. Furthermore, POD algorithms are not always guaranteed to converge, especially if the initial guess given by the IOD is poor. The more precise the initial guess, the higher the performance of the POD in terms of number of iterations required to converge (and speed of convergence). This, again, highlights the cardinal role of Initial Orbit Determination in the OD process. We can therefore state that IOD methods are a field of research as important as ever.

1.2 The history of orbit determination

The first traces of Orbit Determination date back to the first half of the XVII century when Kepler, interpreting the observations made by Tycho Brahe, published the *Tabulae Rudolphinae* [8] in 1627. The study of the accurate measurements made by Brahe has been the basis for the development of the three laws of planetary motion, used to provide, in the tables, a means to evaluate the position of thousands of stars and the known planets. A considerable part of the tables consists in fact of instructions on how to use them and the logarithmic calculus in order to recover the position of a celestial body in a previous or future moment in time. The methods described are applied to many examples in the manuscript itself and were based on the area rule for elliptic orbits (Kepler's second law). These tables served for years as the most precise means to evaluate the positions of planets, stars and comets [9]. Nonetheless, Kepler did not provide any analytical expression to recover the orbit of a body given some observations of it.

The first author of a solution to the OD problem was Newton who, in the *Principia* [10], describes a graphical procedure to recover the parabolic orbit from three observations on a plane [11]. This procedure was then applied by Halley, leading him to the discovery of Halley's comet, but it was difficult to understand and was based on successive graphical approximations. Still, this was not an analytical solution.

After Newton, many mathematicians and astronomers worked on the problem, such as Euler, Lambert, Lagrange, Laplace, Gauss and Gibbs, just to name some of the most famous ones[12]. Euler was the first one to provide an analytical solution to the OD problem. In his work *Theoria motuum planetarum et cometarum* [13], he states in different ways the problem of recovering the orbits given partial knowledge of the orbital elements and some observations. In 1743, he also derived the expression of the parabola passing through two positions given the time-of-flight between them. The same problem was independently solved by Lambert in 1761 for (again) the parabolic case, and in the following decade for

elliptical and hyperbolic orbits [14]. Mathematical elegance to these results was given by Lagrange [15]. This type of IOD, formulated with the use of two position vectors and time-of-flight, is universally referred to as *Lambert's problem*. Recalling the subdivision made in the previous section, all these solutions fall into the class of position-based IODs. The angles-only IOD was instead solved in the first place by Laplace and Gauss. The observations consisted of line of sight (LOS) measurements, so only the direction of the orbiting object's position vector was known. In 1780, Laplace published his solution [16], followed by Gauss in 1809 [17]. The method proposed by Laplace was difficult to apply because of the too heavy computations, and is considered inaccurate for Earth-orbiting satellites [18]. Still widely used, the Gauss method is more reliable for Earth orbiting satellites, but only until the observations are not too spread (some authors suggest no more than $60°$ apart [19]). We complete this brief review of angles-only IOD by mentioning the more recent solution proposed by Escobal [20] in 1965, namely the Double-R method, which works well both for spread and close observations.

We finally recall a method that is different from all the previous ones in that it does not make use of time information to work. It was proposed by Gibbs in 1889 [21] and, starting from three position vectors, gives as output the velocity of the object at one of the three positions, uniquely identifying the orbit.

1.3 Some considerations about the existing IOD methods

Since a lot of IOD solutions have been proposed for all the different formulations, the motivation behind a new approach to the angles-only IOD problem must be given. In Table 1.1 a schematic comparison between the inputs required by some of the most common IOD is shown. Until now, IOD methods have been classified in terms of the type of spatial measurements used, not considering that temporal measurements are also often needed. In fact, time appears among the inputs of almost all the IOD solutions presented in the table, and it has a role in determining the number of measurements necessary to solve the prob-

lem. Therefore, we can expect that for the same type of spatial measurements (for example LOS, or position vector), if time is used then fewer observations will be needed. In the table, we can see that this occurs when comparing Lambert's solution, which only needs two observations, to Gibbs', which needs three observations. Also, if we want to compare the quantity of information enclosed in a LOS measurement, it is clear that a LOS contains less information than that enclosed in a position vector, which additionally contains range information. Along the same line, we can expect that more measurements will be needed if LOS are used, and we can verify this by comparing the solution of Lambert with the solution of Gauss, for example, which uses three observations and time. The aim of this work is to analyze the capability of a new approach first presented in [22], where the angles-only IOD problem is solved without the use of time in any way. Following the reasoning made before, we can therefore expect that this solution, referred to as the homotopy-based solution, requires more observations than the others listed in the table. In fact, it needs five LOS measurements to provide a finite number of solution orbits.

The importance of angles-only IOD is that bearing (direction) information is more easily obtainable than other measurements, since a telescope or a camera are sufficient to gather the observation. Obtaining range information for the determination of the position vector, on the other hand, is not always simple [23]. In fact, range measurements are strictly related to the measurement of time. We can distinguish between the range information obtained by measuring the time taken by a signal to travel from the observer to the satellite and then back to the observer (two-way range), or only using the time taken by the signal to

Table 1.1: Summary of some common IOD formulations

Method	**Gauss & Laplace & Double-R & Gooding**	**Lambert**	**Gibbs**	**Hodograph**	**This work**
Number of observations	3	2	3	3	5
Type of observation	angles	position	position	velocity	angles
Use of time	yes	yes	no	no	no

travel from the observer to the satellite or vice-versa (one-way range). However, both types of range measurements present complexities. In the one-way range, the target satellite must have an onboard clock precisely synchronized with a clock at the observer position. When two bodies have a relative acceleration, relativistic effects cause a difference in the duration of a second for them [24]. Keeping clocks synchronized, for this reason, is a necessary step to provide an accurate measurement of the time difference between when the signal leaves the observer (measured with one clock) and when it reaches the satellite (measured with the other clock). Another factor that influences the precision of the estimate (both for the one-way and the two-way range) is related to the finiteness of the light velocity. During the time taken by the signal to travel from the satellite to the observer, the satellite position will change, since it will continue to move along its own trajectory, and the observation made will be associated to the wrong time instant (so to the wrong position, and the wrong range). A correction can be applied if the distance traveled by the light is known (assuming to ignore other phenomena that influence the signal velocity, like for example changes of the medium of propagation or change of properties of this medium - density, humidity, etc). However, the distance traveled by the light is the range that we are trying to measure, so it is unknown. In an IOD problem, we also assume that no a priori information is available, so estimating the error introduced by the light time-of-flight can be non-trivial, leading to further inaccuracies in the initial orbit estimation process. If the correction is not made, the farther the object, the higher the error.

Clearly, estimating the light time-of-flight is not specific to the range measurement, but it is in general something that we have to take into account when we record the time of any type of observation, including LOS measurements. All the issues listed until now make an IOD solution that does not make use of time or range information attractive, because it would not only simplify the pre-processing corrections of the measurements, but would also significantly decrease the complexity of the instrumentation devoted to the IOD task (no onboard clocks, no necessity to store time information). This would make the IOD

feasible even with the most basic type of instrumentation.

1.4 Organization of the work

The homotopy-based solution analyzed in this work is based on a polynomial reformulation of the equation of the IOD problem obtained using tools from projective geometry. The solution of the final polynomial system was found using a homotopy continuation method. For this reason, the mathematical background for the comprehension of the geometric re-parameterization of the orbit will be first reviewed. Then, the specific reformulation of [22] will be developed and novel paths will be studied that will lead to a geometric interpretation of the constraints imposed to the system.

The further step made in this work is to consider streaks in digital images as inputs to the problem in combination with LOS observations, taking inspiration from [3], keeping the assumption made above on the absence of time-of-flight information and any type of initial guess. Subsequently, a numerical study of the performance of the bearings-only case will be made, and it will be compared with the results provided by a standard IOD solution. This will be followed by an analysis of the results provided by a combination of streaks and LOS measurements. Finally, possible future paths for the development of the work will be discussed.

CHAPTER 2
MATHEMATICAL BACKGROUND

In this chapter, the mathematical tools for the development of the process that leads to the polynomial reformulation of the IOD problem will be given. First, some basic notions of projective geometry will be introduced and then some geometric results used in the rest of this work will be discussed.

Since part of this work is based on the projection of geometric features on a plane, some useful properties of projective geometry of two dimensions will first be presented. From that, similar properties of the projective space will be deduced by analogy, and this will give the necessary tools for the development of the relationship between LOS observations and the orbit as analyzed in the first part of chapter 4. However, the reformulation of the equations of the problem requires the knowledge of how conics and quadrics are treated in projective geometry. For this reason part of this chapter is also devoted to their description.

2.1 Projective geometry: homogeneous coordinates

Projective geometry is usually considered born from the work of Girard Desargues in the XVII century [25], with some notions dating back to the era of Apollonius of Perga [26] (II-III century B.C.) and Pappus (IV century), but it fell out of use shortly after. The new and definitive flowering of projective geometry took place in the XIX century with Jean-Victor Poncelet, the first mathematician who made a systematic study of the subject [27], and it is now recognized as a powerful tool that allows geometric problems to be approached elegantly. I will give a summary of the potentiality of this approach to geometry, with a focus towards the results that have been used to reformulate the IOD problem. For a more complete and formal introduction to the subject, the reader can refer to books like [28] and [29].

Given a vector space $\mathbb{V}^{n+1}$ of dimension $n+1$ over a field $\mathcal{K}$, the projective space $\mathbb{P}^n$ can be defined as the set of one-dimensional subspaces of $\mathbb{V}^{n+1}$ [30]. In other words, we can associate any point of the projective space of dimension n to a one-dimensional subspace of a vector space of dimension $n+1$. Two elements are equivalent in the projective space if they belong to the same vector subspace of the space of higher dimension. From a more practical standpoint, this means that a point in $\mathbb{P}^n$ is described by all the non-zero scalar multiples of a vector with $n+1$ coordinates. A point on the projective line (a point in $\mathbb{P}^1$) is associated to all the points of a one-dimensional subspace of a two-dimensional vector space (a line in the plane - two coordinates). Similarly, points on the projective plane are described with three coordinates and points in the projective space with four. The *homogeneous coordinates* of a point in the projective space $\mathbb{P}^n$ can be easily obtained by appending a 1 to the n-dimensional vector of coordinates of the point in the standard space $\mathbb{R}^n$, if assume $\mathbb{V} = \mathbb{R}$. From now on, when an element is said to be part of the projective space of any dimension, it is tacit that homogeneous coordinates are used.

The interpretation of this additional coordinate is simple when the geometry of $\mathbb{P}^1$ or $\mathbb{P}^2$ is considered, but the principle is the same for the projective geometry of any dimension. There are multiple advantages brought by it, and they will be in part clarified in the next subsections, where we will look at features of projective geometry in two and three dimensions and then at the description of conics and quadrics.

2.2 The projective plane

An extremely intuitive description of projective geometry in two dimensions is given by N. Wildberger [31], and a consistent part of this section takes inspiration from his lectures.

Consider an orthonormal coordinate system in three dimensions, with axis x, y and z, and consider the plane $z = 1$. Also, assume that we fix a coordinate frame for that plane such that the origin is at the intersection with the z-axis and the axes X and Y are parallel to the axes x and y of the three-dimensional frame. A representation of this scenario is

given in Figure 2.1.

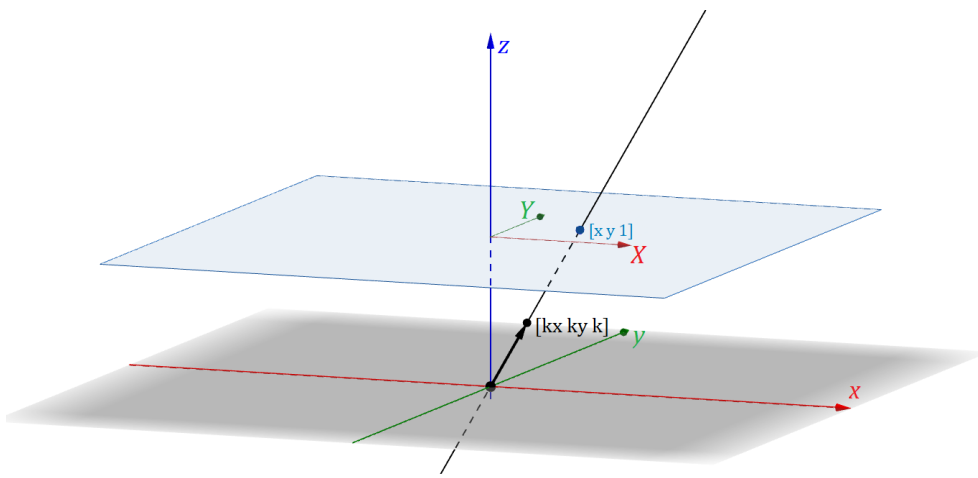

Figure 2.1: Points in the projective plane are described in terms of all the one-dimensional subspaces of the augmented vector space $\mathbb{R}^3$.

Now, take a point in the plane and the line through the origin passing through that point. If the point has coordinates, in the two-dimensional reference frame, given by $\mathbf{x}^T = [X\, Y]$, its coordinates in the three-dimensional frame will be given by $\bar{\mathbf{x}}^T = [\mathbf{x}^T\, 1]$ and any other point on the same line will be described by a scalar multiple of $\bar{\mathbf{x}}$. If we decide to map every point on that line to the point on the plane, then the point on the plane is described by all the non-zero scalar multiples of the vector $\bar{\mathbf{x}}$. In other words, the homogeneous coordinates of the point in the projective plane are given by $\bar{\mathbf{x}}^T \propto [X\, Y\, 1]$ and the coordinates of any point on the line passing through it are acceptable for the description of the point in the projective plane: the points on the projective plane are represented through the direction of the corresponding line in the augmented space.

2.2.1 Points at infinity

Now, imagine to gradually rotate the line through the origin until it lies in the x-y plane, as in Figure 2.2. The point of intersection between the line and the plane, i.e. the point on the projective plane, will move far from the origin, approaching the infinity. When the line completely lies in the x-y plane, the z component of its direction vector becomes zero,

and this reflects the fact that the X and Y components of the corresponding point tend to infinity. This point at infinity is therefore characterized by having the last homogeneous coordinate equal to 0 and it is representative of a direction - the direction of all the lines parallel to the line in the x-y plane. Since we have an infinite number of directions that do not intersect the projective plane (all the lines lying in the x-y plane), there is an infinite number of points at infinity, lying on the so-called line at infinity. The introduction of points at infinity as representative of directions in the projective plane allows the generalization of the axiom that two lines in a plane intersect at a point, even if they are parallel. In this case, the point of intersection will be the common point at infinity associated with their direction.

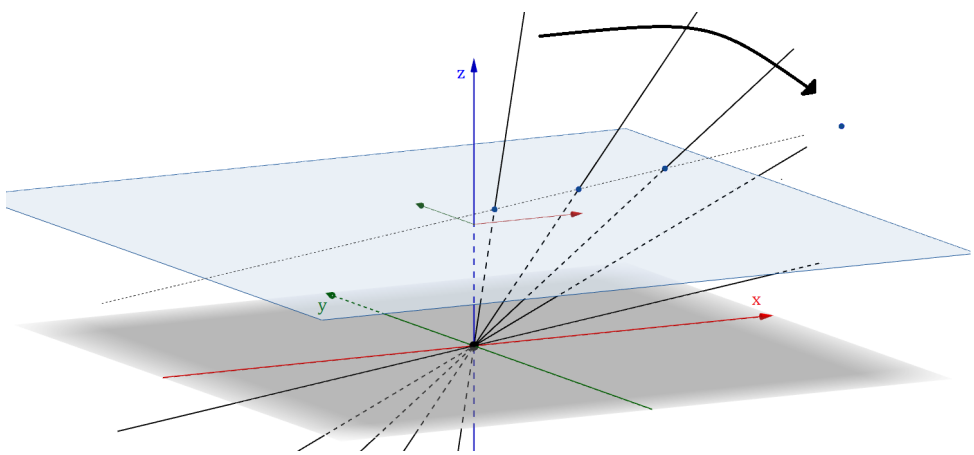

Figure 2.2: As the black line approaches the line in the x-y plane, the point in the projective plane moves to infinity in the direction of the line in the x-y plane.

2.2.2 Duality

Another important consequence of the addition of a coordinate to the world is the notion of duality. The Cartesian equation of a line in the plane is given, in 2D, by

$$aX + bY + c = 0$$

but using homogeneous coordinates, since $X = x/z$ and $Y = y/z$, under the condition that $z \neq 0$, we can rewrite the equation as

$$ax + by + cz = 0$$

or

$$\begin{bmatrix} a & b & c \end{bmatrix} \begin{bmatrix} x \\ y \\ z \end{bmatrix} = 0 \tag{2.1}$$

This means that every line in the projective plane, even if it doesn't pass through the origin, can be described with a homogeneous equation.

Now let $\bar{\mathbf{x}}^T \propto [x\, y\, z]$ and $\boldsymbol{\ell}^T \propto [a\, b\, c]$. The line can be described *directly* in terms of all its points, and *dually* in terms of the line coordinates $\boldsymbol{\ell}$. If we imagine to keep fixed $\boldsymbol{\ell}$, varying $\bar{\mathbf{x}}$ such that Equation 2.1 is satisfied, we obtain all the points lying on the same line $\boldsymbol{\ell}$. If we fix $\bar{\mathbf{x}}$ and vary $\boldsymbol{\ell}$, we obtain the coordinates of all the lines of the pencil with center at $\bar{\mathbf{x}}$. This relation is at the basis of the parallelism between points and lines, which is formally described in the *Principle of Duality* [28]:

If a theorem is valid in the projective geometry of the plane, the dual theorem obtained replacing the word point with the word line, the word collinear with concurrent and the word join with meet, and viceversa, is still valid.

A simple application of this theorem leads to the conclusion that, since the join of two points generates a line (direct theorem), the meet of two lines generates a point (dual theorem). Similarly, we know that if $\bar{\mathbf{x}}_1$ and $\bar{\mathbf{x}}_2$ are two points in $\mathbb{P}^2$, a third collinear point $\bar{\mathbf{x}}_3$ can be obtained as $\bar{\mathbf{x}}_3 \propto \bar{\mathbf{x}}_1 + \lambda \bar{\mathbf{x}}_2$, with $\lambda \in \mathbb{R}$. Dually, if two lines are given by $\boldsymbol{\ell}_1$ and $\boldsymbol{\ell}_2$, a line $\boldsymbol{\ell}_3$ meeting them at their point of intersection has coordinates $\boldsymbol{\ell}_3 \propto \boldsymbol{\ell}_1 + \lambda \boldsymbol{\ell}_2$.

2.2.3 Non-singular linear transformation of $\mathbb{P}^2$

Another consequence of the duality principle is that if $\mathbf{H}$ is a non-singular linear transformation of points in $\mathbb{P}^2$ such that

$$\bar{\mathbf{x}}' = \mathbf{H}\bar{\mathbf{x}} \tag{2.2}$$

and $\boldsymbol{\ell}$ is a line through $\bar{\mathbf{x}}$ ($\boldsymbol{\ell}^T\bar{\mathbf{x}} = 0$), the line $\boldsymbol{\ell}$ transforms as

$$\boldsymbol{\ell}' = \mathbf{H}^{-T}\boldsymbol{\ell} \tag{2.3}$$

and the transformed point $\bar{\mathbf{x}}'$ will still lie on the transformed line $\boldsymbol{\ell}'$ ($\boldsymbol{\ell}'^T\bar{\mathbf{x}}' = 0$).

2.2.4 Join and meet in the projective plane

It is worth mentioning that lines also have a physical interpretation in the augmented space. In fact, the coordinates of a line are the components of a vector normal to the plane passing through the origin of the three-dimensional space, which intersects the projective plane in that line. This can be shown easily if we look at the operation of join of two points. The join of two elements is defined as the smallest subspace containing them. The join of two points is in general a line, and the join of two non-skew (intersecting) lines is a plane. The operation of join is easily performed in homogeneous coordinates. The coordinates of the line passing through two points $\bar{\mathbf{x}}_1$ and $\bar{\mathbf{x}}_2$ of the projective plane, in fact, are given by their cross product:

$$\boldsymbol{\ell} \propto \bar{\mathbf{x}}_1 \times \bar{\mathbf{x}}_2 \tag{2.4}$$

This can be seen moving to the augmented space, looking at Figure 2.3. The join of the two lines which represent the points in the projective plane is a plane, passing through the origin of the augmented space, that also contains the points $\bar{\mathbf{x}}_1$ and $\bar{\mathbf{x}}_2$. This plane intersects the plane $z = 1$ in the line that we want to find. Since its normal vector must be orthogonal to both the lines, it can be found as the cross product between their direction vectors, which

are $\bar{\mathbf{x}}_1$ and $\bar{\mathbf{x}}_2$. Now let ℓ_i be the component of this normal vector $\boldsymbol{\ell} = \bar{\mathbf{x}}_1 \times \bar{\mathbf{x}}_2$. The equation of the plane will be

$$\ell_1 x + \ell_2 y + \ell_3 z = 0 \tag{2.5}$$

However, the coordinates of any point on that plane are the homogeneous coordinates of a point on the line in the projective plane. Since they satisfy Equation 2.5, the components of $\boldsymbol{\ell}$ must also be the homogeneous coordinates of the line joining the two points.

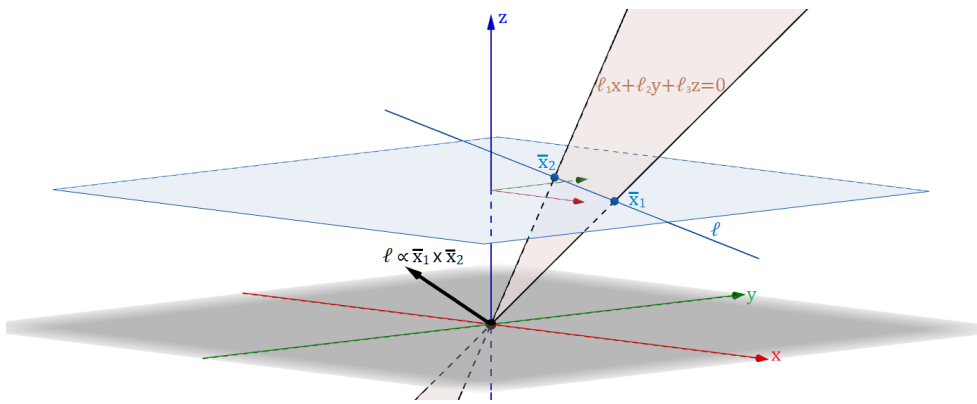

Figure 2.3: The join of two points $\bar{\mathbf{x}}_1$ and $\bar{\mathbf{x}}_2$ is given by the cross product $\boldsymbol{\ell} \propto \bar{\mathbf{x}}_1 \times \bar{\mathbf{x}}_2$.

We can proceed similarly to obtain the expression of the meet of two lines. The meet of two objects is defined as the smallest subspace contained by them. So, the meet of two lines in a plane is a point. Given two lines $\boldsymbol{\ell}_1$ and $\boldsymbol{\ell}_2$, the coordinates of their point of intersection $\bar{\mathbf{x}}$ are given by:

$$\bar{\mathbf{x}} \propto \boldsymbol{\ell}_1 \times \boldsymbol{\ell}_2 \tag{2.6}$$

This can be demonstrated considering the meet of the two planes of the augmented space representing the lines $\boldsymbol{\ell}_1$ and $\boldsymbol{\ell}_2$. This intersection is a line, whose direction vector must be orthogonal to their normal vectors, represented again by $\boldsymbol{\ell}_1$ and $\boldsymbol{\ell}_2$ as seen above, so it is given by their cross product. The direction of this line gives the homogeneous coordinates of the corresponding point in the projective plane. A visualization of the meet is given in Figure 2.4. In summary, the basic operations of meet and join can both be performed using the simple cross product.

Going back and forth from the projective space to the augmented space is particularly useful to understand how the projection works when using a camera since it allows us to relate in a straightforward way what we see in the image plane to what is the real world.

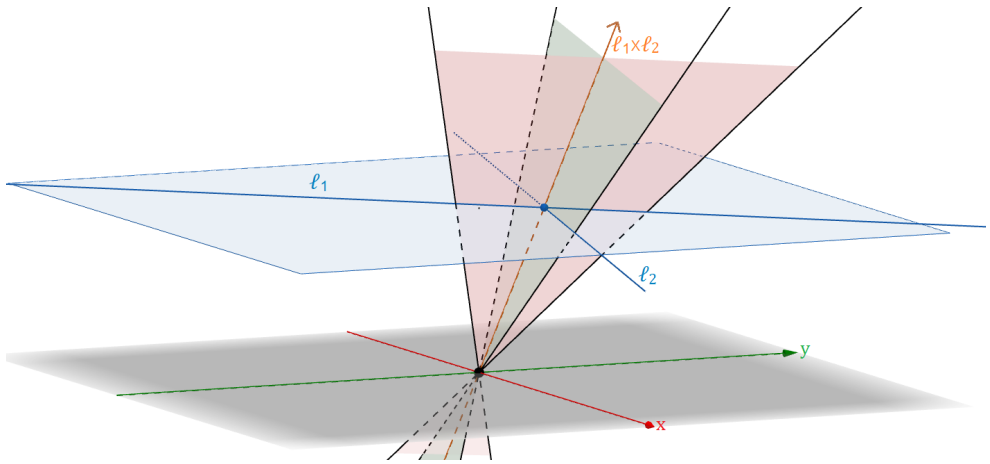

Figure 2.4: The meet of two lines $\boldsymbol{\ell}_1$ and $\boldsymbol{\ell}_2$ is given by the cross product $\bar{\mathbf{x}} \propto \boldsymbol{\ell}_1 \times \boldsymbol{\ell}_2$.

2.2.5 The projective space

When dealing with the projective geometry of three dimensions (or, in general, of more than two dimensions), the meaning of *adding a coordinate* is not simple to visualize. We can imagine that the process is a generalization of what was shown before, and looking at the analytical consequences of it may be more intuitive. A point $\bar{\mathbf{x}} \in \mathbb{P}^3$ is represented through four coordinates as $\bar{\mathbf{x}}^T \propto [X\, Y\, Z\, 1]$. Since the equation of any plane in Cartesian geometry can be given as:

$$aX + bY + cZ + d = 0$$

when using homogeneous coordinates, calling t the extra coordinate, being $X = x/t$, $Y = y/t$, $Z = z/t$, we can rewrite it, under the condition $t \neq 0$ as:

$$ax + by + cz + dt = 0$$

or

$$\begin{bmatrix} a & b & c & d \end{bmatrix} \begin{bmatrix} x \\ y \\ z \\ t \end{bmatrix} = 0 \tag{2.7}$$

Also in this case we can associate to a plane $\boldsymbol{\pi}$ its coordinates $\boldsymbol{\pi}^T \propto [a\,b\,c\,d]$ and establish a duality relationship between points and planes of the projective space. Fixing the plane $\boldsymbol{\pi}$, all the points of that plane must have coordinates $\bar{\mathbf{x}}^T \propto [x\,y\,z\,t]$ such that Equation 2.7 is satisfied. Fixing $\bar{\mathbf{x}}$, all the planes with coordinates $\boldsymbol{\pi}$ such that Equation 2.7 is satisfied are instead the planes of the star with center at $\bar{\mathbf{x}}$.

2.2.6 Duality and points at infinity

The principle of duality in $\mathbb{P}^3$ is analogous to that enunciated in $\mathbb{P}^2$, where planes are used instead of lines. If a theorem is given directly in terms of points, it can be restated dually in terms of planes, keeping in mind that lines are self-dual in $\mathbb{P}^3$. As before, then, if the join of two points is a line, the meet of two planes is a line. Similarly, given two points on a line $\bar{\mathbf{x}}_1$ and $\bar{\mathbf{x}}_2$, a third point $\bar{\mathbf{x}}_3$ along the same line can be obtained as a linear combination of the first two. Dually, given two planes $\boldsymbol{\pi}_1$ and $\boldsymbol{\pi}_2$, any third plane $\boldsymbol{\pi}_3$ meeting the previous two at the same line can be obtained as $\boldsymbol{\pi}_3 \propto \boldsymbol{\pi}_2 + \lambda\boldsymbol{\pi}_2$ for some $\lambda \in \mathbb{R}$.

Also in this case, when $t = 0$ we obtain a point at infinity, and all the points at infinity lie on the plane at infinity $\boldsymbol{\pi}_\infty \propto [0\,0\,0\,1]^T$. Any two parallel planes always meet in a line on that plane.

2.2.7 Non-singular linear transformation of $\mathbb{P}^3$

As in the projective plane, if $\mathbf{H}$ is the matrix associated to a non-singular transformation of the projective space, i.e. $\bar{\mathbf{x}}' \propto \mathbf{H}\bar{\mathbf{x}}$, and if $\boldsymbol{\pi}^T\,\bar{\mathbf{x}} = 0$, the plane coordinates will be

transformed accordingly by

$$\boldsymbol{\pi}' = \mathbf{H}^{-T}\boldsymbol{\pi} \tag{2.8}$$

and the transformed plane $\boldsymbol{\pi}'$ will contain the transformed point $\bar{\mathbf{x}}'$.

2.2.8 Lines in $\mathbb{P}^3$

Since the final objective is to study the geometry of an angles-only IOD problem, which is closely linked to the geometry of lines and conics in space, it is of interest to address how lines are represented in the projective space. In $\mathbb{P}^3$, a line can be described directly as given by all its points, or dually as the meet of two planes. If $\bar{\mathbf{x}}_1$ and $\bar{\mathbf{x}}_2$ are two points in $\mathbb{P}^3$ lying on the line $\boldsymbol{\ell} \in \mathbb{P}^3$, all the points on the line lie in the column space of the matrix:

$$\begin{bmatrix} \bar{\mathbf{x}}_1 & \bar{\mathbf{x}}_2 \end{bmatrix} \tag{2.9}$$

Dually, we can describe the line using any 4×2 matrix $\mathbf{A}$ having as columns two planes passing through that line. For the matrix $\mathbf{A}$ to be a suitable representation, then, the following equations must be satisfied

$$\mathbf{A}^T \begin{bmatrix} \bar{\mathbf{x}}_1 & \bar{\mathbf{x}}_2 \end{bmatrix} = \mathbf{0}_{2\times 2} \tag{2.10}$$

This fixes the four degrees of freedom of the line in space. Each column of the matrix $\mathbf{A}$ represents a plane passing through the points $\bar{\mathbf{x}}_1$ and $\bar{\mathbf{x}}_2$ and each of those equations forces one plane to pass through one point $\bar{\mathbf{x}}_1$ or $\bar{\mathbf{x}}_2$. Note that, as described above, any other plane through that line is given by a linear combination of the columns of $\mathbf{A}$:

$$\boldsymbol{\pi} = \mathbf{A}\mathbf{c} \tag{2.11}$$

where $\mathbf{c}$ is a 2×1 vector. This way of describing any plane of a pencil with fixed axis $\boldsymbol{\ell}$ will be particularly important in the development of the constraint relating the orbit to the

observations.

2.3 Conics and quadrics in projective geometry

We know from Cartesian geometry that a conic in a plane is described by a polynomial equation of degree two in two variables, with a general equation of the form:

$$aX^2 + bY^2 + 2cX + 2dY + 2eXY + f = 0 \tag{2.12}$$

Using homogeneous coordinates, if we let $\bar{\mathbf{x}}^T \propto [X\,Y\,1]$, the previous equation can be rewritten in matrix form as:

$$\bar{\mathbf{x}}^T \mathbf{C} \bar{\mathbf{x}} = 0 \tag{2.13}$$

where $\mathbf{C}$ is the symmetric 3×3 matrix associated up to a scalar to the conic:

$$\mathbf{C} \propto \begin{bmatrix} a & e & d \\ e & b & c \\ d & c & f \end{bmatrix} \tag{2.14}$$

and the proportionality symbol has been used because any multiplication of the matrix $\mathbf{C}$ for a scalar does not change the roots of the equation, and does not change the conic.

Equation 2.13 gives the direct description of the conic, since it is satisfied by all the points lying on it. In the projective plane, however, the conic can be also described dually. The dual of a conic is called conic envelope, and it is formed by all the lines that are tangent to the conic at each point, as represented in Figure 2.5. This dual locus is described by an homogeneous quadratic equation. To obtain this equation, we start from the expression of a line tangent to the conic described in terms of a simple product for the matrix $\mathbf{C}$, following the derivation in [29].

Take the point $\bar{\mathbf{x}}_1$ lying on the conic and consider the line $\boldsymbol{\ell} \propto \mathbf{C}\bar{\mathbf{x}}_1$. If we assume that this line intersects the conic also in any other point $\bar{\mathbf{x}}_2$, the following conditions are valid:

- $\bar{\mathbf{x}}_2$ lies on the line $\mathbf{C}\bar{\mathbf{x}}_1$: $\bar{\mathbf{x}}_2^T\mathbf{C}\bar{\mathbf{x}}_1 = 0$
- $\bar{\mathbf{x}}_2$ lies on the conic: $\bar{\mathbf{x}}_2^T\mathbf{C}\bar{\mathbf{x}}_2 = 0$
- $\bar{\mathbf{x}}_1$ lies on the conic: $\bar{\mathbf{x}}_1^T\mathbf{C}\bar{\mathbf{x}}_1^T = 0$

A direct consequence is that the following equation must be valid for any $k \in \mathbb{R}$:

$$(\bar{\mathbf{x}}_1^T + k\bar{\mathbf{x}}_2^T)\mathbf{C}(\bar{\mathbf{x}}_1 + k\bar{\mathbf{x}}_2) = 0 \tag{2.15}$$

but since $\boldsymbol{\ell}$ passes through $\bar{\mathbf{x}}_1$ and $\bar{\mathbf{x}}_2$, $\bar{\mathbf{x}}_1 + k\bar{\mathbf{x}}_2$ gives another point on $\boldsymbol{\ell}$. Equation 2.15 can be then translated into requiring that any point on the line $\boldsymbol{\ell}$ lies on the conic. This is impossible, unless the conic is degenerate. For this reason, the only point of intersection between the line $\boldsymbol{\ell}$ and the conic must be $\bar{\mathbf{x}}_1$, and consequently $\boldsymbol{\ell}$ is tangent to the conic.

We can now derive the equation of the conic envelope. Given the line $\boldsymbol{\ell} \propto \mathbf{C}\bar{\mathbf{x}}$ tangent to the conic at $\bar{\mathbf{x}}$, we can write $\bar{\mathbf{x}} \propto \mathbf{C}^{-1}\boldsymbol{\ell}$ and substitute its expression in Equation 2.13:

$$\boldsymbol{\ell}^T\mathbf{C}^{-T}\mathbf{C}\mathbf{C}^{-1}\boldsymbol{\ell} = 0 \tag{2.16}$$

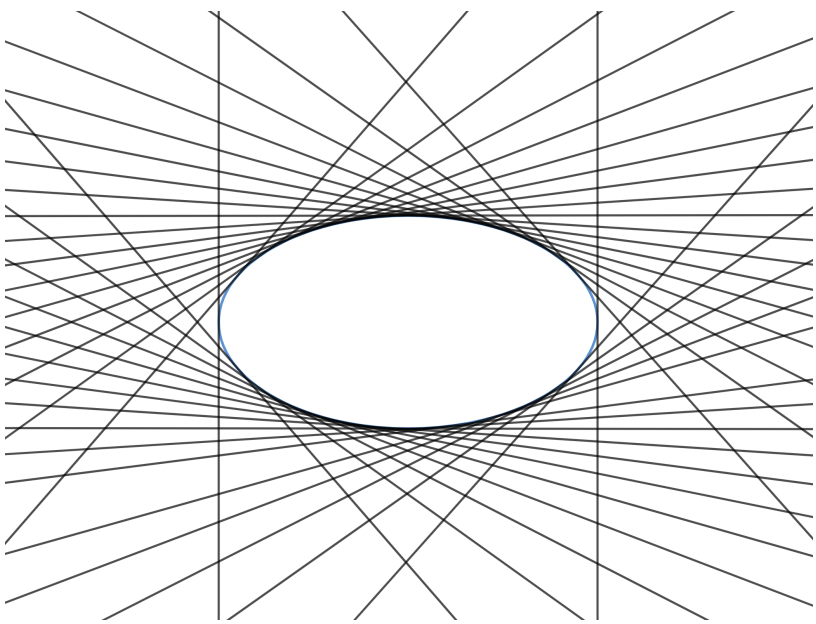

Figure 2.5: All the lines tangent to the conic form its conic envelope.

Recalling the symmetry of $\mathbf{C}$, this provides the equation of the conic envelope

$$\boldsymbol{\ell}^T \mathbf{C}^* \boldsymbol{\ell} = 0 \tag{2.17}$$

where $\mathbf{C}^* \propto \mathbf{C}^{-1}$.

2.3.1 Pole and polar

At this point, a reference to the notions of pole and polar must be done. These concepts date back to the ancient Greeks (II-III century B.C.), when Apollonius of Perga made a huge work in the study of conics [26]. The pole-polar relationship is an orthogonality relationship when the metric is defined through the scalar product given by the symmetric bilinear form associated to the matrix of the considered conic. In other words, we can define the scalar product between two point $\bar{\mathbf{x}}_1$ and $\bar{\mathbf{x}}_2$ as given by the symmetric bilinear form:

$$\mathbb{R}^{n+1} \times \mathbb{R}^{n+1} \rightarrow \mathbb{R}$$

$$< \bar{\mathbf{x}}_1 \, \bar{\mathbf{x}}_2 >= \bar{\mathbf{x}}_1^T \mathbf{C} \bar{\mathbf{x}}_2$$

Given a point $\bar{\mathbf{x}}$ in the plane and a conic described by $\mathbf{C}$, its *polar line* $\boldsymbol{\ell}$ is the line that contains all the points orthogonal to $\bar{\mathbf{x}}$ with respect to the conic. Since orthogonality is satisfied if the scalar product is zero, the polar line has coordinates $\boldsymbol{\ell} \propto \mathbf{C}\bar{\mathbf{x}}$. If $\boldsymbol{\ell}$ is the polar line of the point $\bar{\mathbf{x}}$, then $\bar{\mathbf{x}}$ is said to be the *pole* of the line $\boldsymbol{\ell}$, defined as the meet of all the polar lines of the points on $\boldsymbol{\ell}$ [28]. Given the line $\boldsymbol{\ell}$, its pole $\bar{\mathbf{x}}$ will be $\bar{\mathbf{x}} \propto \mathbf{C}^* \boldsymbol{\ell}$. Note the similarity between the expression of the polar line of a point and the tangent line through a point on the conic. The polar line of a point on the conic is in fact the line tangent to the conic at that point.

A visualization of the geometric construction of the polar line of a point is given in Figure 2.6. In this figure we can see how the polar line of a point can be obtained joining

the intersections between the two tangents drawn from that point and the conic. In fact, since the orthogonality relationship is commutative, if $\bar{\mathbf{x}}_2$ is a point on the polar line $\boldsymbol{\ell}$ of $\bar{\mathbf{x}}_1$, then $\bar{\mathbf{x}}_1$ must be a point of the polar line of $\bar{\mathbf{x}}_2$. But if we choose $\bar{\mathbf{x}}_2$ on the conic, its polar is also the tangent to the conic. Since this must be valid for both the points where the line meets the conic, the two tangents at the intersection points of $\boldsymbol{\ell}$ with the conic must meet at $\bar{\mathbf{x}}_1$. Now, imagine to move the point $\bar{\mathbf{x}}_1$ progressively closer to the conic, as in Figure 2.7. As the point approaches the conic, the two points of contact of the tangent line drawn from $\bar{\mathbf{x}}_1$ get closer, until they become coincident when $\bar{\mathbf{x}}_1$ meets the conic. So, as a point approaches a conic, we expect its distance from its polar line to decrease. This fact will be relevant in the geometric interpretation of the algebraic constraint of the IOD system of equations.

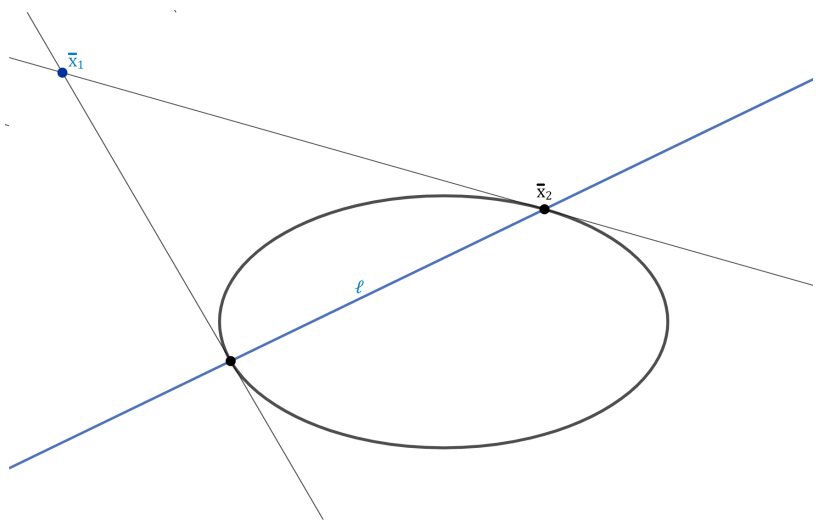

Figure 2.6: The polar line $\boldsymbol{\ell}$ of a point $\bar{\mathbf{x}}_1$ joins the points of tangency of the two tangents drawn from $\bar{\mathbf{x}}_1$.

Now, we can move to the three-dimensional space. As done in two dimensions, we can give a direct and a dual description of the conic. When working in $\mathbb{P}^3$, a homogeneous quadratic equation produces a quadric surface [28]. A conic can be described directly as all the points of intersection between a quadric, for example a cone, and a plane. The dual description is usually easier to treat. It is given by all the planes that are tangent to the conic at each point. This locus of planes takes the name of *disk quadric* and it has been sketched

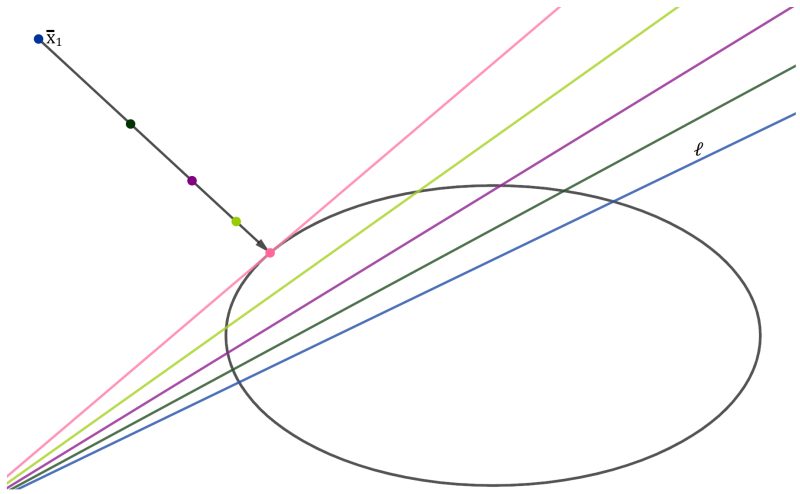

Figure 2.7: As the point approaches the conic, the distance from its polar line decreases.

in Figure 2.8. All the planes that belong to this locus must satisfy another homogeneous quadratic equation

$$\boldsymbol{\pi}^T \mathbf{Q}^* \boldsymbol{\pi} = 0 \tag{2.18}$$

where $\mathbf{Q}^*$ is a symmetric 4×4 matrix of rank three, defined up to a scalar. A full rank $\mathbf{Q}^*$ matrix would in fact produce the quadric envelope of a non-degenerate quadric. We can think to the space conic as a quadric that flattens until it looses one dimension. Note that there are eight independent coefficients in Equation 2.18. In other words, eight planes in general position uniquely identify a disk quadric - or a space conic. The Keplerian orbit of an object in space can therefore be described through a 4×4 matrix defining, up to a scalar, the associated disk quadric.

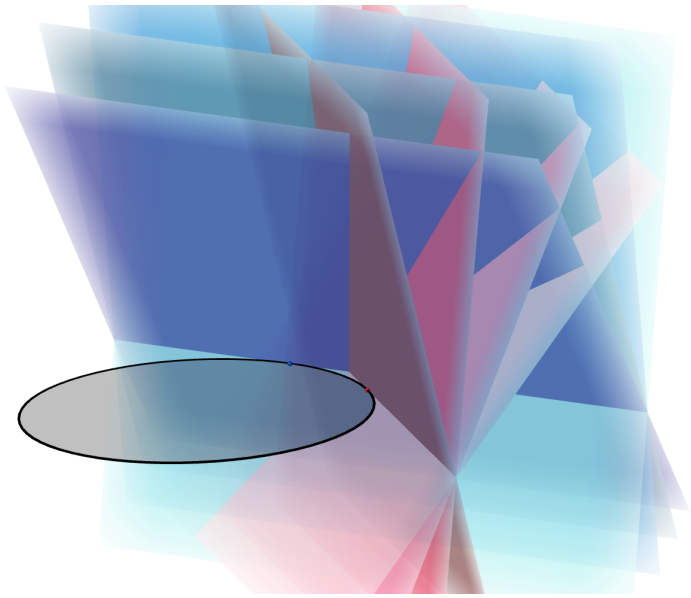

Figure 2.8: All the planes tangent to the space conic define a locus, the *disk quadric*

CHAPTER 3

THE ORBIT IN HOMOGENEOUS COORDINATES

This work is based on the assumption of Keplerian dynamics. For this reason, the dynamical equations of the problem will be first recalled, together with the final expression of the equation of motion. After that, a link between the classical elements used to describe an orbit and the corresponding expression of the disk quadric will be made, developing the reformulation of the orbit already used in [22].

3.1 The dynamical model

Consider two bodies in space only subjected to their mutual attraction, which can be modeled with an inverse-square gravity model. This approximation is valid when the mass of the two bodies is spherically distributed, or when the two bodies are significantly away one from the other, so that they produce the gravitational attraction of point-masses placed at their centers of mass. Let the body with bigger mass M be the main or primary body. The other body is the secondary body, and has mass m. In any inertial reference frame, letting $\mathbf{r}_1$ and $\mathbf{r}_2$ be respectively the position vectors of the main and secondary body, $\boldsymbol{\rho} = \mathbf{r}_2 - \mathbf{r}_1$ the vector going from the first to the second, and G the gravitational constant, we can write the forces acting on the two bodies as

$$\mathbf{f}_1 = \frac{G\,M\,m}{\rho^3}\boldsymbol{\rho} \tag{3.1a}$$

$$\mathbf{f}_2 = -\frac{G\,M\,m}{\rho^3}\boldsymbol{\rho} \tag{3.1b}$$

and their equations of motion as

$$\ddot{\mathbf{r}}_1 = \frac{G\,m}{\rho^3}\boldsymbol{\rho} \tag{3.2a}$$

$$\ddot{\mathbf{r}}_2 = -\frac{G\,M}{\rho^3}\boldsymbol{\rho} \tag{3.2b}$$

The motion of the secondary body with respect to the main one can be obtained subtracting Equation 3.2b from Equation 3.2a:

$$\ddot{\mathbf{r}}_2 - \ddot{\mathbf{r}}_1 = \ddot{\boldsymbol{\rho}} = -\frac{G\,(m+M)}{\rho^3}\boldsymbol{\rho} \tag{3.3}$$

Now, assume that the mass of the main body is significantly greater than the secondary one's ($M >> m$). This assumption is legitimate for example for a satellite orbiting a planet. The previous equation takes the form

$$\ddot{\boldsymbol{\rho}} = -\frac{\mu}{\rho^3}\,\boldsymbol{\rho} \tag{3.4}$$

where $\mu = G\,M$ is the gravitational parameter of the central body.

The general solution to this second-order differential equation is:

$$\rho(t) = \frac{p}{1 + e\,cos(\nu(t))} \tag{3.5}$$

where p and e are respectively the semi-latus rectum and the eccentricity of the conic and $\nu(t)$ is the true anomaly angle, localizing the spacecraft on the orbit at a certain time t.

It can be demonstrated that Equation 3.5 is a parametrization of the distance of the points on a conic from one of its foci [32]. This restricts the possible orbits that can be traveled in the two body problem to conic sections - ellipse, parabola and hyperbola. Starting from this result, the orbit is a space conic and it can be associated with its disk quadric.

From now on, the words ”conic” and ”orbit” will be interchangeably used, and it will be assumed that the orbit is closed - the conic is an ellipse.

3.1.1 The perifocal reference frame

Given an object (say a spacecraft) in orbit around a main body (a planet), the perifocal reference frame $(O, \{\mathbf{p}, \mathbf{q}, \mathbf{w}\})$ can be uniquely defined. This reference frame has origin O at the center of mass of the planet with p-axis pointing towards the pericenter of the orbit, w-axis along the angular momentum vector of the spacecraft, and q-axis in the orbital plane, completing the right-handed triad (see Figure 3.1). This reference frame is fixed and independent of the position of the spacecraft along the orbit. An important consideration is that the two vectors of the basis **p** and **q** span the orbital plane, but the orbital plane can be also identified solely by the vector **w**, although the last provides less information since we have no clues on the orientation of the orbit in the plane, which is instead given by **p** or **q**. On the other hand, as the orbit becomes more and more circular, the eccentricity $e = c/a$ tends to zero, and the pericenter of the orbit, defined as the closest point to the focus, is no longer defined. This is an important problem in the use of the perifocal frame for the description of the orbit, and will be addressed in detail later in the next section.

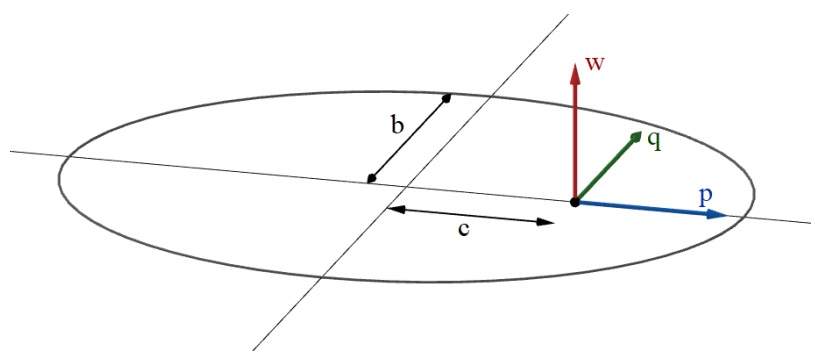

Figure 3.1: The perifocal frame.

3.2 The orbit as a disk quadric

Repeating the steps in [22], the description of the orbit in terms of its disk quadric will now be given. In the orbital plane defined by the axes p and q, the orbit is completely described by two parameters that fix the size and shape of the orbit. The parameters usually considered are the semi-major axis *a* and the eccentricity *e*, but other choices can be made. For example, another option is to use the semi-major axis, the semi-minor axis *b* and the focal length *c* of the conic, recalling that these parameters are interrelated and related to the eccentricity by the relations:

$$a^2 = b^2 + c^2 \tag{3.6a}$$

$$c = ea \tag{3.6b}$$

The simplest expression of the ellipse in the perifocal frame is then:

$$\frac{(X+c)^2}{a^2} + \frac{Y^2}{b^2} = 1 \tag{3.7}$$

With few manipulations, considering Equation 3.6a, Equation 3.7 can be written in matrix form, using homogeneous coordinates in $\mathbb{P}^2$

$$\bar{\mathbf{s}}^T \mathbf{C} \bar{\mathbf{s}} = 0 \tag{3.8}$$

where

$$\mathbf{C} \propto \begin{bmatrix} b^2 & 0 & b^2 c \\ 0 & a^2 & 0 \\ b^2 c & 0 & -b^4 \end{bmatrix} \tag{3.9}$$

and $\bar{\mathbf{s}}^T \propto [X\, Y\, 1]$.

As seen in section 2.3 we can also describe an ellipse in the plane in a dual manner

through its envelope, and write the following expression for the matrix associated with it

$$\mathbf{C}^* \propto \mathbf{C}^{-1} \propto \begin{bmatrix} 1 & 0 & c/b^2 \\ 0 & 1 & 0 \\ c/b^2 & 0 & -1/b^2 \end{bmatrix} \tag{3.10}$$

where we recall

$$\boldsymbol{\ell}^T \mathbf{C}^* \boldsymbol{\ell} = 0 \tag{3.11}$$

However, the conic is in a general position in space, so we need to move from this planar description to the three-dimensional one. The assumption made is that the center of the reference frame remains at the focus of the conic. A way to look at this shift is to consider the transformation matrix that performs the change of coordinates from the perifocal frame to the inertial frame, considering the three-dimensional orientation of the vectors $\mathbf{p}$ and $\mathbf{q}$. Note that a point $\bar{\mathbf{s}} \in \mathbb{P}^2$ expressed in the p-q frame is related to its three-dimensional description $\bar{\mathbf{x}}_P \in \mathbb{P}^3$ in the perifocal frame by

$$\bar{\mathbf{x}}_P = \begin{bmatrix} 1 & 0 & 0 \\ 0 & 1 & 0 \\ 0 & 0 & 0 \\ 0 & 0 & 1 \end{bmatrix} \bar{\mathbf{s}} = \boldsymbol{\Gamma} \bar{\mathbf{s}} \tag{3.12}$$

The matrix that provides the change of coordinates from the perifocal frame to the inertial frame has columns containing the components of the perifocal frame vectors expressed in the inertial frame. Let $\bar{\mathbf{H}}$ be this matrix

$$\bar{\mathbf{H}} = \begin{bmatrix} \mathbf{p} & \mathbf{q} & \mathbf{w} & \mathbf{0}_{3\times 1} \\ 0 & 0 & 0 & 1 \end{bmatrix} \tag{3.13}$$

where the last column accounts for the zero-translation of the origin and the last row trans-

forms the directions of $\mathbf{p}$, $\mathbf{q}$ and $\mathbf{w}$ in $\mathbb{R}^3$ to points at infinity of $\mathbb{P}^3$. This matrix provides the transformation

$$\bar{\mathbf{x}} \propto \bar{\mathbf{H}}\,\bar{\mathbf{x}}_P = \bar{\mathbf{H}}\,\boldsymbol{\Gamma}\,\bar{\mathbf{s}} = \mathbf{H}\,\bar{\mathbf{s}} \tag{3.14}$$

In conclusion, the change of coordinates from the p-q plane (the orbital plane) to the inertial frame is given by

$$\mathbf{H} = \begin{bmatrix} \mathbf{p} & \mathbf{q} & \mathbf{0}_{3\times 1} \\ 0 & 0 & 1 \end{bmatrix} \tag{3.15}$$

and we have

$$\bar{\mathbf{x}} \propto \mathbf{H}\,\bar{\mathbf{s}} \tag{3.16}$$

This matrix $\mathbf{H}$ is the matrix of the direct transformation of points in the projective space. If we repeat the whole process for the matrix of the dual transformation $\bar{\mathbf{H}}^{-T}$ (see subsection 2.2.7) we can obtaian a relation between a line $\boldsymbol{\ell}$ in the orbit plane and any plane $\boldsymbol{\pi}$ passing through it:

$$\boldsymbol{\ell} \propto \mathbf{H}^T \boldsymbol{\pi} \tag{3.17}$$

where $\mathbf{H}$ is of rank three and $\boldsymbol{\pi}$ has one degree of freedom.

From the final expression of Equation 3.17 we can infer that this kind of transformation from $\mathbb{P}^2$ to $\mathbb{P}^3$ will transform any line tangent to the conic (any line of the conic envelope) into a pencil of planes with axis that line (the planes of the disk quadric), providing at the same time a change of coordinates from the perifocal frame to the inertial frame. Substituting Equation 3.17 into Equation 3.11 we arrive to the final equation of the disk quadric:

$$\boldsymbol{\pi}^T\,\mathbf{H}\,\mathbf{C}^*\,\mathbf{H}^T\,\boldsymbol{\pi} = 0 \tag{3.18}$$

Finally, the disk quadric is described by the 4×4 symmetric matrix $\mathbf{Q}^*$ given by:

$$\mathbf{Q}^* \propto \mathbf{H}\mathbf{C}^*\mathbf{H}^T \tag{3.19}$$

3.2.1 Parameterizations of the disk quadric

The substitution of the matrix $\mathbf{H}$ in Equation 3.19 gives the following explicit expression of the disk quadric, first appeared in [3]:

$$\mathbf{Q}^* \propto \begin{bmatrix} \mathbf{p}\mathbf{p}^T + \mathbf{q}\mathbf{q}^T & (c/b^2)\mathbf{p} \\ (c/b^2)\mathbf{p}^T & -1/b^2 \end{bmatrix} \tag{3.20}$$

as a function of the perifocal basis vectors $\mathbf{p}$ and $\mathbf{q}$, and of the two in-plane parameters of the ellipse b and c. However, as already noted earlier, this parameterization can cause issues. In fact, in the case of a circular orbit, the eccentricity of the conic is zero and the pericenter becomes undefined. Since nearly-circular orbits are frequent, especially for Earth-orbiting satellites, this problem cannot be ignored. The solution used in [22] was the following. First, since $\mathbf{w} = \mathbf{p} \times \mathbf{q}$, the following relation holds:

$$\mathbf{p}\mathbf{p}^T + \mathbf{q}\mathbf{q}^T = \mathbf{I}_3 - \mathbf{w}\mathbf{w}^T \tag{3.21}$$

Also, if we rename $\mathbf{g} = c/b^2\mathbf{p}$, the problem of the undefiniteness is solved. In fact, when the eccentricity goes to zero, the linear eccentricity $e \to 0$ and the vector $\mathbf{g} \to \mathbf{0}_{3\times1}$ remains defined. Since we have no more explicit dependency on the vectors $\mathbf{p}$ and $\mathbf{q}$ of the perifocal base, this parameterization is always well defined.

In conclusion, the following parameterization of the disk quadric should therefore be preferred:

$$\mathbf{Q}^* \propto \begin{bmatrix} \mathbf{I}_3 - \mathbf{w}\mathbf{w}^T & \mathbf{g} \\ \mathbf{g}^T & -1/b^2 \end{bmatrix} \tag{3.22}$$

The disk quadric has now been expressed as a function of seven unknowns, so seven equations are needed to solve for it. However, since the vectors $\mathbf{w}$ and $\mathbf{p}$ are vectors of the perifocal frame, which is orthonormal, and since $\mathbf{g}$ is parallel to $\mathbf{p}$, two equations are

already given:

$$\mathbf{w}^T\mathbf{w} - 1 = 0 \tag{3.23a}$$

$$\mathbf{w}^T\mathbf{g} = 0 \tag{3.23b}$$

Five additional equations are needed to solve for the unknowns inside $\mathbf{Q}^*$, and these equations will come from the LOS observations. Once this polynomial system with seven equations and seven unknowns is solved, we obtain a description of the orbit as a disk quadric, in homogeneous coordinates. Given the matrix $\mathbf{Q}^*$, the classical orbital elements can be easily recovered. Note that since the matrix $\mathbf{Q}^*$ is independent of the sign of $\mathbf{w}$. If we do not introduce any assumption on the direction of motion, the longitude of the node Ω and the argument of the pericenter ω will be recovered with an ambiguity of π.

CHAPTER 4

THE EQUATIONS OF THE BEARINGS-ONLY IOD PROBLEM

The objective of this chapter is to develop the polynomial system of equations of the IOD problem. This has to be done relating the observations to the unknowns contained in the disk quadric. When the observations consist of LOS (bearing) measurements, the information is usually given in terms of position of the observer and right ascension and declination. Recovering the unit vector in the inertial frame associated with these angles is a standard procedure. Assuming that this step has already been done, the setup of the problem can be expressed in the following way: n lines in general position in space, representing the lines of sight of n observations, intersect a space conic at unknown distance from the observer - the objective is to recover this conic. This scenario is represented schematically in Figure 4.1.

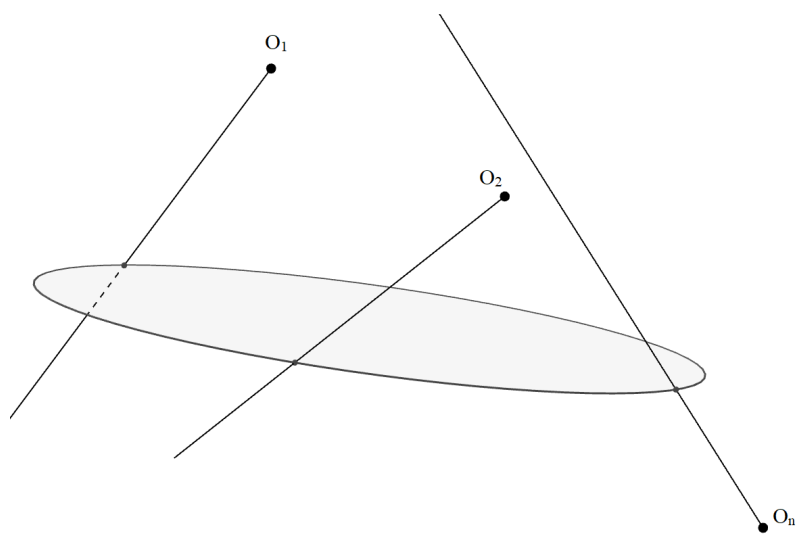

Figure 4.1: Lines of sight corresponding to different observations intersect the orbit at unknown distances from the observers O_i.

There are different ways to approach the problem of expressing this intersection relation between the LOS and the orbit. I am going to present three of them to show how the same

problem can be solved and approached from different standpoints, which will finally turn out to be equivalent. The first approach has already been used in a previous work presented at the AAS/AIAA Astrodynamics Specialist Conference (Charlotte 2022) [22], and consists of an algebraic constraint of tangency, while the other two are more ”geometric” in the sense that they are based on the zeroing of a geometric distance.

4.1 Algebraic constraint

This approach is based on a three-dimensional analysis of the geometry of the problem. Consider a single observation, with the associated LOS. Even if the position of the intersection point with the orbit is unknown, we know that the point of intersection is unique (unless the observation is coplanar with the orbital plane). This means that we can always build a plane containing the LOS that is tangent to the orbit - in other words, a plane of the disk quadric. This plane is spanned by the LOS and the tangent to the orbit in the orbital plane and it is unique for each observation (see Figure 4.2). This geometric characteristic can be translated into a polynomial equation using homogeneous coordinates.

Consider a single LOS and let $\mathbf{x} \in \mathbb{R}^3$ be the coordinates of the observer and $\mathbf{u} \in \mathbb{R}^3$ the unit vector parallel to the LOS. In homogeneous coordinates, they correspond to the points with coordinates:

$$\bar{\mathbf{x}}^T = \begin{bmatrix} \mathbf{x}^T & 1 \end{bmatrix} \tag{4.1}$$

$$\bar{\mathbf{u}}^T = \begin{bmatrix} \mathbf{u}^T & 0 \end{bmatrix} \tag{4.2}$$

with the second being a point at infinity (see subsection 2.2.6). In subsection 2.2.8 we have seen that the line joining these two points (the LOS) can be represented in the dual space through any 4×2 matrix $\mathbf{A}$ such that

$$\mathbf{A}^T \begin{bmatrix} \bar{\mathbf{x}} & \bar{\mathbf{u}} \end{bmatrix} = \mathbf{0}_{2\times 2} \tag{4.3}$$

Again, we recall that any other plane passing through the LOS can be written as

$$\boldsymbol{\pi} = \mathbf{A}\,\mathbf{c} \tag{4.4}$$

where $\mathbf{c}$ is a 2×1 vector. This plane $\boldsymbol{\pi}$ belongs to the disk quadric if:

$$\mathbf{c}^T\,\mathbf{A}^T\,\mathbf{Q}^*\,\mathbf{A}\,\mathbf{c} = 0 \tag{4.5}$$

which is equivalent to requiring that the 2×2 matrix $\mathbf{A}^T\mathbf{Q}^*\mathbf{A}$ is rank deficient:

$$det\left|\mathbf{A}^T\mathbf{Q}^*\mathbf{A}\right| = 0 \tag{4.6}$$

This equation represents a polynomial constraint that relates the unknowns (inside $\mathbf{Q}^*$) to the observation (encoded in $\mathbf{A}$). For n observations, we can specify Equation 4.6 for

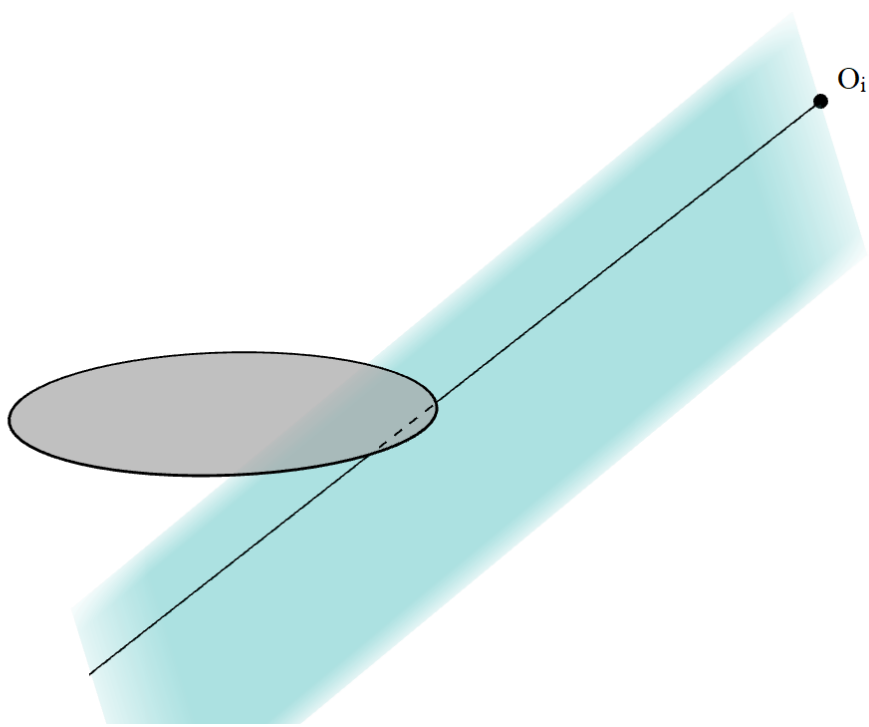

Figure 4.2: There is a unique plane of the disk quadric that contains the LOS generated by an observer.

each of them and obtain n polynomial constraints:

$$det \left|\mathbf{A}_i^T \mathbf{Q}^* \mathbf{A}_i\right| = 0 \qquad i = 1 \dots n \tag{4.7}$$

that together with Equation 3.23a and Equation 3.23b form a polynomial system of $n + 2$ equations. Since the unknowns are seven, *five* observations are needed to obtain a finite number of solutions for the system.

The choice of **A** is free as far as its columns are two planes passing through the LOS. Below, an analytic and a numeric way to obtain this matrix are addressed.

*Definition of the **A** matrix*

As already mentioned, there are several ways to build the **A** matrix, and there are several ways to relate the observations to the disk quadric. We mention here one of the valid analytical expressions, and one numeric derivation of it, as in [22]. Let the 2×2 matrices $\mathbf{S}_1$ and $\mathbf{S}_2$ be defined such that:

$$\begin{bmatrix} \mathbf{S}_1 & \mathbf{S}_2 \end{bmatrix} = \begin{bmatrix} \mathbf{x} & \mathbf{u} \\ 1 & 0 \end{bmatrix} \tag{4.8}$$

We can write the **A** matrix as:

$$\mathbf{A} = \begin{bmatrix} \mathbf{A}_0 & -\mathbf{A}_0 \mathbf{S}_1 \mathbf{S}_2^{-1} \end{bmatrix} \tag{4.9}$$

where $\mathbf{A}_0$ is any invertible 2×2 matrix. A simple choice is $\mathbf{A}_0 = u_3 \mathbf{I}_{2\times 2}$. In this way, we obtain:

$$\mathbf{A} = \begin{bmatrix} u_3 & 0 \\ 0 & u_3 \\ u_1 & u_2 \\ x_1 u_3 - x_3 u_1 & x_2 u_3 - x_3 u_2 \end{bmatrix} \tag{4.10}$$

The parameters inside this matrix can be specified for each observation.

The other approach, which has been implemented in the analysis of the results, is numeric and is the following. Since the matrix $\mathbf{A}$ must satisfy Equation 4.3, it must also satisfy the transposed equation

$$\begin{bmatrix} \bar{\mathbf{x}}^T \\ \bar{\mathbf{u}}^T \end{bmatrix} \mathbf{A} = \mathbf{0}_{2\times 2} \tag{4.11}$$

Through the singular value decomposition (SVD) we obtain

$$\begin{bmatrix} \bar{\mathbf{x}}^T \\ \bar{\mathbf{u}}^T \end{bmatrix} = \mathbf{U}\mathbf{\Sigma}\mathbf{V}^T \tag{4.12}$$

Since

$$\mathbf{\Sigma} = \begin{bmatrix} \sigma_1 & 0 \\ 0 & \sigma_2 \\ 0 & 0 \\ 0 & 0 \end{bmatrix} \tag{4.13}$$

given that $\mathbf{A}$ must lie in the null space of the transposed primal matrix $[\bar{\mathbf{x}}\,\bar{\mathbf{u}}]^T$, if we let $\mathbf{v}_i$ be the columns of the matrix $\mathbf{V}$, we can evaluate $\mathbf{A}$ as

$$\mathbf{A} = \begin{bmatrix} \mathbf{v}_3 & \mathbf{v}_4 \end{bmatrix}^T \tag{4.14}$$

4.2 In-plane constraints

With the objective of finding the expression of a quantity that, if minimized, provides some intuition of the accuracy of the estimation, another way to arrive to the same polynomial constraint of Equation 4.6 has been found that may provide an interpretation of the polynomial constraint imposed. This reformulation also allows us to easily determine the degree of that equation.

The approach is based on the projection of the orbit on n image planes, that correspond to the image planes of $n_c \leq n$ fictitious or real cameras gathering the observations. For the moment, consider a camera providing a bearing measurement. Let $\mathbf{T}$ be the rotation matrix representing the attitude of the camera frame with respect to the inertial frame and let $\mathbf{x} \in \mathbb{R}^3$ be the camera location. If $\mathbf{r} \in \mathbb{R}^3$ is the position of the spacecraft when imaged by the camera, the direction of observation in the inertial frame is $\mathbf{u} = \mathbf{r} - \mathbf{x}$. Recalling the interpretation of points in the projective plane given in section 2.2, we can write the homogeneous coordinates $\bar{\mathbf{s}}$ of a point in the image plane of the camera, expressed in the camera frame, as the coordinates of the direction vector of the line along $\mathbf{u}$ expressed in the camera frame:

$$\bar{\mathbf{s}} \propto \mathbf{u}_C = \mathbf{r}_C - \mathbf{x}_C = \mathbf{T}\left(\mathbf{r} - \mathbf{x}\right) \tag{4.15}$$

which provides the homogeneous coordinates of the intersection between the image plane and the line joining the camera with the observed point. So a generic point in space with inertial coordinates $\mathbf{r}$ is transformed to the point $\bar{\mathbf{s}}$ by the transformation:

$$\bar{\mathbf{s}} \propto \left[\mathbf{T} \ -\mathbf{T}\mathbf{x}\right] \begin{bmatrix} \mathbf{r} \\ 1 \end{bmatrix} \tag{4.16}$$

This projection is represented in Figure 4.3.

The matrix $\mathbf{P}$ is called *camera projection matrix*:

$$\mathbf{P} = \mathbf{T}\left[\mathbf{I}_3 \ -\mathbf{x}\right] \tag{4.17}$$

and provides the mapping $\mathbb{P}^3 \rightarrow \mathbb{P}^2$ from points in the space ($\bar{\mathbf{r}}^T \propto [\mathbf{r} \ 1]$) to points on the image plane ($\bar{\mathbf{s}}$):

$$\bar{\mathbf{s}} \propto \mathbf{P}\bar{\mathbf{r}} \tag{4.18}$$

Also points at infinity in $\mathbb{P}^3$ (i.e. directions) can be mapped to finite points on the image

plane (when taking a picture of a landscape, the horizon - line at infinity - is a finite line on the image). Then if we want to map the point at infinity associated with the direction of the actual LOS, $\mathbf{u}$, we obtain the corresponding point in the image plane $\bar{\mathbf{s}}_0$

$$\bar{\mathbf{s}}_0 \propto \mathbf{u}_C \tag{4.19}$$

Note that the coordinates of the point $\bar{\mathbf{s}}_0$ are known, since that is the point imaged by the camera when the satellite is sighted.

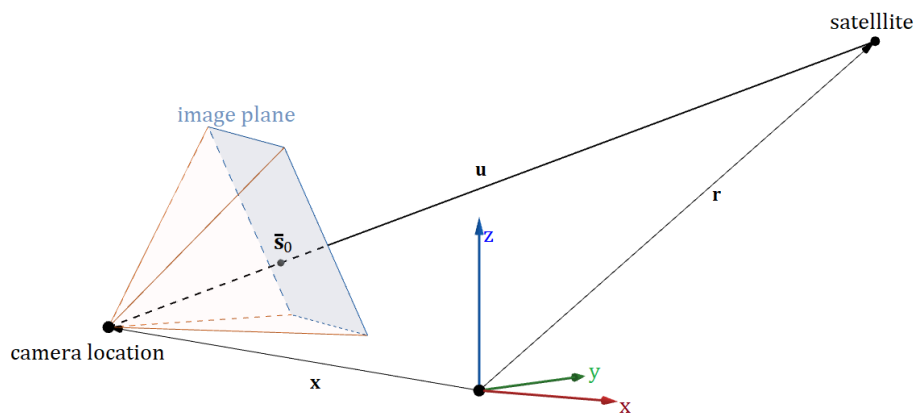

Figure 4.3: Visualization of the projection of the position of the satellite on the image plane of a camera.

If the conic was an actual object in space and the camera imaged all its point at the same time, the collection of all the lines of sight would create a cone in space, that intersects the image plane in a conic, as represented in Figure 4.4.

Similarly, the conic envelope in the orbit plane would project to a conic envelope in the image plane, created by the intersection with the image plane of all the planes of the disk quadric containing the observer. These planes are also tangent to the cone created by the LOS, as illustrated in Figure 4.5. The disk quadric projects then on the image plane as a conic envelope. This projection is ruled by the projection matrix $\mathbf{P}$. Since the relation

between the imaged line $\boldsymbol{\ell}$ and the plane of the disk quadric $\boldsymbol{\pi}$ is

$$\boldsymbol{\pi} \propto \mathbf{P}^T \boldsymbol{\ell} \tag{4.20}$$

substituting into the equation of the disk quadric we obtain

$$\boldsymbol{\ell}^T \, \mathbf{P} \, \mathbf{Q}^* \, \mathbf{P}^T \, \boldsymbol{\ell} = 0 \tag{4.21}$$

where we can rename the matrix

$$\mathbf{C}_C^* \propto \mathbf{P}\mathbf{Q}^*\mathbf{P}^T \tag{4.22}$$

representing the conic envelope in the image plane. After some manipulations we obtain an expression that will be useful in the study of the degree of the polynomial equation:

$$\mathbf{C}_C^* = [\mathbf{T}\mathbf{T}^T - \mathbf{T}\,\mathbf{w}\,\mathbf{w}^T\,\mathbf{T}^T - \mathbf{T}\mathbf{x}(\mathbf{T}\,\mathbf{g})^T - \mathbf{T}\,\mathbf{g}\,(\mathbf{T}\mathbf{x})^T + \mathbf{T}\mathbf{x}\,(\mathbf{T}\mathbf{x})^T/b^2] \tag{4.23}$$

We now have an expression for the projected conic envelope on the image plane as a function of the unknowns $(\mathbf{w}, \mathbf{g}, b)$, and the given point $\bar{\mathbf{s}}_0$, which must belong to it. Our objective is to find a polynomial constraint that imposes the passage of the projected conic through that point.

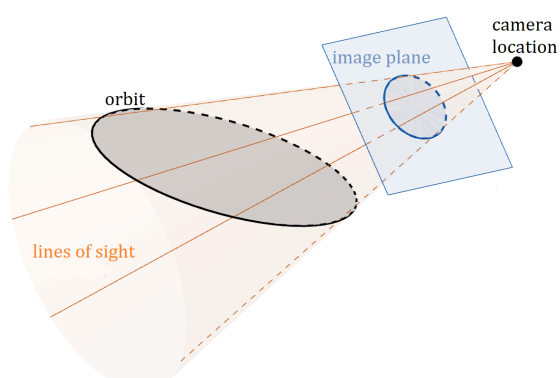

Figure 4.4: The orbit lies on the surface of a cone with vertex at the observer, that intersect the image plane in another conic.

4.2.1 Dual approach

The first possibility is to directly use the dual description of the conic just described. Working in the image plane, consider the conic envelope described by the matrix $\mathbf{C}_C^*$ and the imaged point $\bar{\mathbf{s}}_0$ corresponding to an observation. In the ideal case, this point belongs to the conic, and a general line through it, say $\boldsymbol{\ell}_1$, intersects the conic in two points.

If we let

$$\bar{\mathbf{s}}_0^T \propto \begin{bmatrix} s_1 & s_2 & s_3 \end{bmatrix} \tag{4.24}$$

a simple choice for $\boldsymbol{\ell}_1$ can be

$$\boldsymbol{\ell}_1^T \propto \begin{bmatrix} s_3 & 0 & -s_1 \end{bmatrix} \tag{4.25}$$

Now, take the pole of $\boldsymbol{\ell}_1$:

$$\bar{\mathbf{s}}_1 \propto \mathbf{C}_C^* \boldsymbol{\ell}_1 \tag{4.26}$$

The line $\boldsymbol{\ell}_0$ joining this point and the point $\bar{\mathbf{s}}_0$ must be tangent to the conic (see subsection 2.3.1), as represented in Figure 4.6. This line can be obtained as:

$$\boldsymbol{\ell}_0 \propto \bar{\mathbf{s}}_0 \times \bar{\mathbf{s}}_1 \tag{4.27}$$

Finally, let $\hat{\bar{\mathbf{s}}}_0$ be the pole of this line:

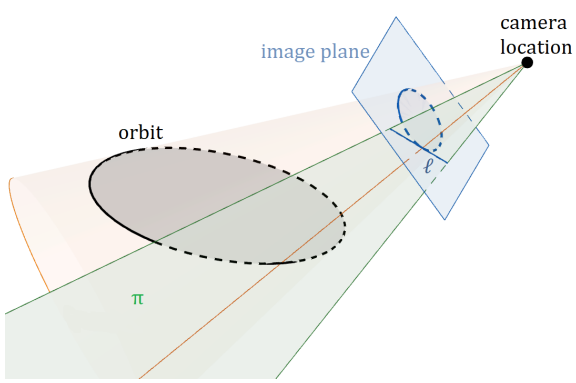

Figure 4.5: The plane of the orbit's disk quadric that contains the observer projects to a line of the conic envelope in the image plane.

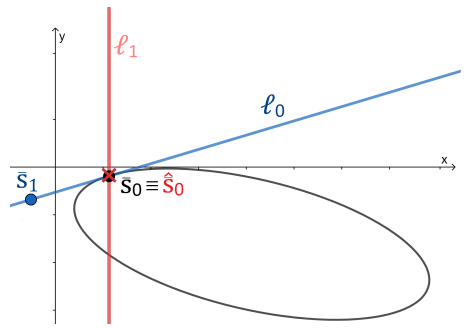

Figure 4.6: The tangent to the conic at one point must pass through the pole of any line passing through that point.

$$\hat{\bar{\mathbf{s}}}_0 \propto \mathbf{C}_C^* \boldsymbol{\ell}_0 \tag{4.28}$$

Note that for the commutativity of the pole-polar relationship (see subsection 2.3.1), the point $\hat{\bar{\mathbf{s}}}_0$ is constrained to lie on $\boldsymbol{\ell}_1$ independenlty of the position of $\bar{\mathbf{s}}_0$ with respect to the conic.

If the imaged point lies exactly on the conic $\hat{\bar{\mathbf{s}}}_0$ and $\bar{\mathbf{s}}_0$ coincide. Then:

$$\hat{\bar{\mathbf{s}}}_0 \times \bar{\mathbf{s}}_0 = \mathbf{0}_{3\times 1} \tag{4.29}$$

For a generic choice of the line $\boldsymbol{\ell}_1$, two of the three equations above are linearly dependent. We can extract a single equation form that condition imposing that the distance between the points $\bar{\mathbf{s}}_0$ and $\hat{\bar{\mathbf{s}}}_0$ is zero in the image plane:

$$d^2 = \left(\frac{s_1}{s_3} - \frac{\hat{s}_1}{\hat{s}_3}\right)^2 + \left(\frac{s_2}{s_3} - \frac{\hat{s}_2}{\hat{s}_3}\right)^2 \tag{4.30}$$

If the point $\bar{\mathbf{s}}_0$ lies on the conic, this distance is zero for any choice of the line $\boldsymbol{\ell}_1$. However, if we choose $\boldsymbol{\ell}_1$ as in Equation 4.25, since it is a line parallel to the y-axis of the camera frame, then $s_1 = \hat{s}_1$ and the expression of their distance simplifies to

$$d = \left(\frac{s_2}{s_3} - \frac{\hat{s}_2}{\hat{s}_3}\right) \tag{4.31}$$

Setting it to zero, we can write the polynomial constraint as:

$$\left(\frac{s_2}{s_3}\hat{s}_3 - \hat{s}_2\right) = 0 \tag{4.32}$$

This constraint can be proved to be equivalent to that imposed by Equation 4.6. The quantity on the left-hand side, however, no longer represents the distance between the points $\bar{\mathbf{s}}_0$ and $\hat{\bar{\mathbf{s}}}_0$ in the image plane. It is the distance between these points when projected on the plane $z = \hat{s}_3$. This plane is different for any position of the camera, for any direction of observation, and depends on the estimated orbit. Minimizing a cost-function given by the sum of the quantity on the left-hand side of Equation 4.32 specified for each observation is therefore not necessarily optimal in terms of finding the best fit conic that minimizes those distances in the image planes.

Note that when the point $\bar{\mathbf{s}}_0$ does not lie on the conic, the three points $\bar{\mathbf{s}}_0$, $\bar{\mathbf{s}}_1$ and $\hat{\bar{\mathbf{s}}}_0$ are the vertices of a self-polar triangle for the conic (see Figure 4.7): each side of the triangle is on the polar line of the opposite vertex. Since each conic has ∞^3 self-polar triangles [28], a further study of the properties of self-polar triangles may be of interest to understand whether the expression of the distance can be simplified or it could make sense minimizing some other geometric quantity. In fact, requiring that the points $\bar{\mathbf{s}}_0$ and $\hat{\bar{\mathbf{s}}}_0$ coincide means imposing that any self polar triangle with one vertex at $\bar{\mathbf{s}}_0$ must be degenerate.

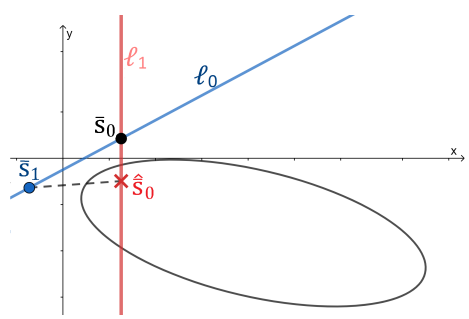

Figure 4.7: When the point $\bar{\mathbf{s}}_0$ does not lie on the conic, the distance between the points $\bar{\mathbf{s}}_0$ and $\hat{\bar{\mathbf{s}}}_0$ is non-zero.

Note that the degree of the polynomial constraint cannot be changed by any non-

singular linear change of coordinates in the image plane. So any attitude represented by the matrix **T**, excluding singular configurations, may only lead to a change of the coefficients of the polynomial. However, the factorization and normalization of the polynomials given by Equation 4.32 and by Equation 4.6 shows that they are equivalent, so the contribution of the attitude matrix **T** can be factored out.

A particular choice of the matrix **T**, however, is useful to show that the polynomial constraint is not of degree four, as expected, but it is of degree three. In fact, assume that the attitude of the camera is such that the z-axis of the camera frame is aligned with the LOS. Then

$$\bar{\mathbf{s}}_0^T \propto \begin{bmatrix} 0 & 0 & 1 \end{bmatrix} \tag{4.33}$$

and a choice for $\boldsymbol{\ell}_1$ can be the y-axis:

$$\boldsymbol{\ell}_1^T \propto \begin{bmatrix} 1 & 0 & 0 \end{bmatrix} \tag{4.34}$$

If we let

$$\mathbf{C}_C^* = \begin{bmatrix} C_{11} & C_{12} & C_{13} \\ C_{12} & C_{22} & C_{23} \\ C_{13} & C_{23} & C_{33} \end{bmatrix} \tag{4.35}$$

we can write the pole of the line $\boldsymbol{\ell}_1$ as

$$\bar{\mathbf{s}_1} \propto \mathbf{C}_C^* \boldsymbol{\ell}_1 = \begin{bmatrix} C_{11} \\ C_{12} \\ C_{13} \end{bmatrix} \tag{4.36}$$

and we can choose the line $\boldsymbol{\ell}_0$

$$\boldsymbol{\ell}_0 \propto \begin{bmatrix} -C_{12} \\ C_{11} \\ 0 \end{bmatrix} \tag{4.37}$$

The guessed point $\hat{\bar{\mathbf{s}}}_0$ will be

$$\hat{\bar{\mathbf{s}}}_0 \propto \begin{bmatrix} 0 \\ C_{11}C_{22} - C_{12}^2 \\ C_{11}C_{23} - C_{12}C_{13} \end{bmatrix} \tag{4.38}$$

Since we want this point to be at the origin of the camera frame, the polynomial of Equation 4.32 reduces to

$$C_{12}^2 - C_{11}C_{22} = 0 \tag{4.39}$$

Analyzing the expression for $\mathbf{C}_C^*$ of Equation 4.23, we see that the higher order terms are given by the multiplication of terms inside the matrix

$$\mathbf{M} = \mathbf{T}\mathbf{w}\mathbf{w}^T\mathbf{T}^T \tag{4.40}$$

The product

$$M_{11}M_{22} - M_{12}^2 \tag{4.41}$$

inside Equation 4.39 is the only one that can produce terms of degree four inside Equation 4.39. The expansion of these terms however shows that we cannot have terms of order higher than three. In fact:

$$M_{11} = T_{11}w_1 + T_{12}w_2 + T_{13}w_3$$

$$M_{22} = (T_{11}w_1 + T_{12}w_2 + T_{13}w_3)(T_{21}w_1 + T_{22}w_2 + T_{23}w_3)$$

$$M_{12} = T_{21}w_1 + T_{22}w_2 + T_{23}w_3$$

and consequently

$$M_{11}M_{22} - M_{12}^2 = 0 \tag{4.42}$$

The results obtained can be summarized as follows. First, the polynomial constraint imposed has been shown being of degree three. Also, the minimization of the algebraic constraint of Equation 4.6 doesn't necessarily produce the best fit conic of the points imaged by the cameras, with the best estimate defined in terms of the distance between the imaged point and the pole of line that, in the ideal case, would be tangent to the conic at the imaged point.

4.2.2 Direct approach

Using the same framework described above, in this section we use the relationship $\mathbf{C}_C \propto \mathbf{C}_C^{*-1}$ to obtain the symmetric 3×3 matrix associated, up to a scalar, to the point equation of the conic in the image plane. At this point we can directly impose the condition that the point $\bar{\mathbf{s}}_0$ must lie on it:

$$\bar{\mathbf{s}}_0^T \, \mathbf{C}_C \, \bar{\mathbf{s}}_0 = 0 \tag{4.43}$$

From basic Euclidean geometry of the plane, we know that the distance between a point with coordinates (X_p, Y_p) and a line with equation $aX + bY + c = 0$ is given by:

$$d = \frac{aX_p + Y_p + c}{(a^2 + b^2)^{1/2}} \tag{4.44}$$

which is proportional to the product of the line and point coordinates in homogeneous coordinates: $d \propto [x_p \, y_p \, 1][a \, b \, c]^T$. We can therefore interpret the constraint of Equation 4.43 as setting to zero the distance between the point $\bar{\mathbf{s}}_0$, and its polar line $\mathbf{C}_C \, \bar{\mathbf{s}}_0$. Note that this approach requires the inversion of the matrix $\mathbf{C}_C^*$, producing a matrix $\mathbf{C}_C$ with terms at most of degree 4 in the unknowns. Any other manipultion of the equation in the direct description would produce a polynomial constraint of the same degree, or higher.

4.3 Relationship between the different polynomial constraints

The motivation that led to the development of multiple ways to approach the same problem was to try to give a geometrical interpretation of what the polynomial constraint imposed. Searching for a geometric quantity to minimize and possibly simplifying the polynomial constraint was the objective of this section. What has been found is that the three polynomial constraints presented are all equivalent. In fact the complete development and normalization of the equations led to the same polynomial of degree three in the unknowns. Its terms have been reported in Appendix A. The insight that can be drawn from this result is that the ellipse found using the algebraic constraint of Equation 4.6 zeroes the distance between a point and a line that in the ideal case would pass through that point. However, when noise is introduced and more than five observations are used, we can expect that not all the imaged points will lie on the projected conics. The polynomial on the left-hand side of Equation 4.6, is not representative of the distance between the imaged point and the corresponding line on the image plane. Therefore, finding the ellipse that minimizes the sum of the squared values of that polynomial for each observation does not give, in general, the optimal solution. Further studies are in progress to understand how an optimal cost function can be obtained.

CHAPTER 5

USE OF STREAKS AND LINES OF SIGHT

When an object is in the field of view of the camera for a short time interval, it produces a streak on the image. This streak has a direct relationship with the disk quadric and can be exploited in a straightforward manner. The main realization used has already been pointed out in [3]: the observer and the streak define a plane which, in the ideal case, is tangent to the conic, so it belongs to the disk quadric. Consider one observer and a sequence of LOS close together. The intersections of the lines of sight with the image plane define a curve which is approximately a segment of line parallel to the velocity vector of the satellite - the streak (see Figure 5.1). The shorter the observation time, the more the curve approaches a straight line. Consequently, the surface described in space by the lines of sight approaches the plane in Figure 4.5, that we can see is a plane of the disk quadric.

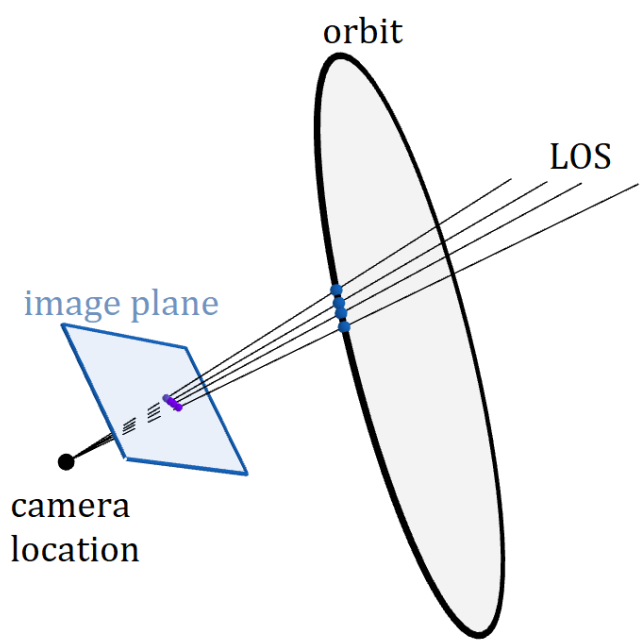

Figure 5.1: The lines of sight collected in a short interval of time create a streak on the image plane.

So, assume we have multiple points on the image plane and we know the coordinates of the best fit line $\boldsymbol{\ell} \in \mathbb{P}^2$ in that plane. Recalling the considerations of subsection 2.2.5 and the initial part of section 4.2 for the development of the in-plane constraints, the plane $\boldsymbol{\pi} \in \mathbb{P}^3$ containing the streak $\boldsymbol{\ell}$ and the observer can be obtained as

$$\boldsymbol{\pi} \propto \mathbf{P}^T \boldsymbol{\ell} \tag{5.1}$$

Since this is a plane of the disk quadric, it must satisfy

$$\boldsymbol{\pi}^T \mathbf{Q}^* \boldsymbol{\pi} = 0 \tag{5.2}$$

or, equivalently,

$$\boldsymbol{\ell}^T \, \mathbf{C}_C^* \, \boldsymbol{\ell} = 0 \tag{5.3}$$

with $\mathbf{C}_C^*$ given in Equation 4.22.

However, this is only one of the two ways in which a streak can be used to constrain the disk quadric. In fact, as done in [3], we can assume that the streak is parallel to the velocity of the satellite at the midpoint of the streak itself. Certain conditions of observations make this assumption more inaccurate than others, but for short observations this is expected to be practically irrelevant, at least in the case of ideal measurements. If we let $\bar{\mathbf{s}}_m$ be the midpoint of the streak $\boldsymbol{\ell}$, we have

$$\bar{\mathbf{s}}_m \propto \mathbf{C}_C^* \, \boldsymbol{\ell} \tag{5.4}$$

From this relation, we can obtain two linearly independent equations. Repeating the steps made in [3], consider the duplication matrix $\mathbf{D}$ such that vec($\mathbf{Q}^*$)= $\mathbf{D}\boldsymbol{\xi}$, where $\boldsymbol{\xi}$ contains the unique entries of $\mathbf{Q}^*$. The unknown scale factor in Equation 5.4 can be removed considering that

$$\bar{\mathbf{s}}_m \times \bar{\mathbf{s}}_m \propto \bar{\mathbf{s}}_m \times \mathbf{C}_C^* \, \boldsymbol{\ell} = \mathbf{0} \tag{5.5}$$

Introducing the Kronecker product $\otimes$, the previous equation can be re-written as

$$[\bar{\mathbf{s}}_m \times] \left(\boldsymbol{\ell}^T \mathbf{P} \otimes \mathbf{P}\right) \mathbf{D}\xi = \mathbf{0}_{3\times 1} \tag{5.6}$$

where we have omitted the use of the calibration matrix of the camera.

This constraint is linear in the entries of $\mathbf{Q}^*$ (contained in $\boldsymbol{\xi}$) and produces the two linearly independent equations we were looking for. However, note that this constraint is not independent of the previous constraint of Equation 5.3. To understand how much the assumption of the midpoint being the projection of the point of tangency to the conic influences the accuracy of the solution, both the *line-to-plane* constraint of Equation 5.3 and the *point-to-point* constraint of Equation 5.6 have been used in the analysis of the results.

5.1 The polynomial system

Let n_{LOS} be the number of LOS observations. Also, assume that n_{PP} is the number of streaks used to impose the point-to-point constraints and n_{LP} is the number of streaks used to impose the line-to-plane constraint. The numbers n_{LOS}, n_{PP} and n_{LP} can be varied as long as $n_{LOS} + 2n_{PP} + n_{LP} = 5$. Depending on the combination of these three numbers, the final polynomial system will be different:

$$\begin{cases} det|\mathbf{A}_i^T \mathbf{Q}^* \mathbf{A}_i| = 0 & \text{for} \quad i = 1, .., n_{LOS} \\ [\bar{\mathbf{s}}_{m,i} \times] \left(\boldsymbol{\ell}_i^T \mathbf{P}_i \otimes \mathbf{P}_i\right) vec(\mathbf{Q}^*) = \mathbf{0}_{3\times 1} & \text{for} \quad i = 1, ..., n_{PP} \\ \boldsymbol{\ell}_i^T \mathbf{C}_{C,i}^* \boldsymbol{\ell}_i = 0 & \text{for} \quad i = 1, ..., n_{LP} \end{cases} \tag{5.7}$$

Note that only two of the three constraints obtained for the *point-to-point* relationship are linearly dependent.

CHAPTER 6

THE POLYNOMIAL SYSTEM OF THE IOD PROBLEM

In the previous chapters various ways to approach the problem of determining the orbit from line of sight observations and streaks on digital images has been addressed. In this chapter, a summary of the procedure to follow when these types of inputs are available will be given, together with a general description of the homotopy used to solve the final system of equations.

Algorithm 1 Polynomial system

```
  if n_LOS > 0 then
      for i = 1 to i = n_LOS do
Require: u_i , x_i
          evaluate A_i                                  ▷ using Equation 4.10
          f_i = det(|A_i^T Q* A_i|)
      end for
  end if
  if n_PP > 0 then
      for i = 1 to i = n_PP do
Require: ℓ_i , x_i , T_i , s̄_{m,i}
          P = T_i − T x_i
          C* = P Q* P^T
          f_{n_LOS+i} = [s̄_m ×](ℓ^T P × P) vec(Q*)
      end for
  end if
  if n_LP > 0 then
      for i = 1 to i = n_LP do
Require: ℓ_i , x_i , T_i
          P = T_i − T_i x_i
          C*_C = P Q* P^T
          f_{n_LOS+n_PP+i} = ℓ_i^T C*_C ℓ_i
      end for
  end if
```

Once the polynomial system $\mathcal{F} = (f_1, ..., f_n)$ has been built, the following step is to find its solution. To do that, a homotopy continuation method has been used. The rest of

this chapter is devoted to an overview of the basic principles of the homotopy used.

6.1 The homotopy continuation

A homotopy continuation method is a tool from algebraic geometry particularly convenient in the resolution of polynomial systems. Although the logic behind the different types of homotopies is easy to understand, there are several hidden aspects that make its implementation cumbersome.

Let $\mathcal{F} = (f_1, ..., f_n) \in \mathbb{C}[\mathbf{x}]^n$ be a polynomial system with complex coefficients, and let it be square, i.e. the number of independent variables is equal to the number of polynomial equations: $\mathbf{x} = (x_1, ..., x_n)$. Also, assume that this system is 0-dimensional, so its variety (set of solutions) has finite dimension. The idea at the basis of any homotopy continuation method is that we can choose a polynomial system $\mathcal{G}$ (the *start system*), whose solution set is known, such that it can be smoothly deformed to make it coincide with the system $\mathcal{F}$, the *target system*. Tracking the paths of the solutions of $\mathcal{G}$ in the process, we will finally be able to numerically recover the solutions of our target system. In order to perform this tracking, the introduction of an extra polynomial system is necessary. Let $\mathcal{H}$ be this auxiliary polynomial system:

$$\mathcal{H}(t) = (1-t)\mathcal{G} + t\mathcal{F}, \qquad t \in [0, 1] \tag{6.1}$$

where the real parameter t takes the name of *continuation parameter*. Note that being $\mathcal{H}(0) \equiv \mathcal{G}$ and $\mathcal{H}(1) \equiv \mathcal{F}$, the solutions of this parametric system coincide with the solutions of the start system when $t = 0$ and with the solutions of the target system when $t = 1$. Since the roots of $\mathcal{H}(0)$ are known, and we want to study how they evolve as the parameter t changes, another equation can be obtained differentiating Equation 6.1 with respect to t:

$$\frac{d\mathcal{H}}{dt} = \frac{\partial \mathcal{H}(t)}{\partial \mathbf{x}} \frac{\partial \mathbf{x}}{\partial t} + \frac{\partial \mathcal{H}(t)}{\partial \mathbf{x}} = 0 \qquad \forall t \tag{6.2}$$

The tracking of the solution set **x** can be made using any predictor-corrector method, where the predictor step is made numerically integrating Equation 6.2 (a classical choice is the Runge-Kutta integration method) and the corrector step is made refining the solution given by the predictor step using a numerical approach like Newton's method applied to Equation 6.1. This process is initialized using the known solutions of the $\mathcal{G}$ system, and it is represented in Figure 6.1 for a 1D system. At the end of the tracking, when $t = 1$, we obtain an estimate of the solutions of the target system.

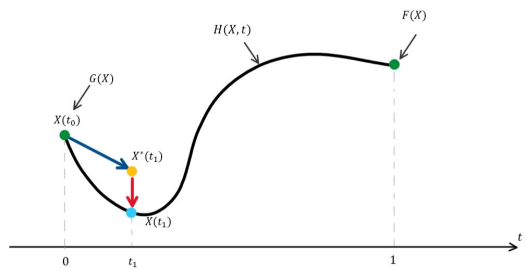

Figure 6.1: As the parameters t goes from 0 to 1, the solutions of the start system $\mathcal{G}$ are deformed into the solutions of the target system $\mathcal{F}$.

6.1.1 Different types of homotopies

The choice of the start system is a fundamental step in the implementation of any homotopy continuation method. It is not required at all that the start system physically or mathematically resembles the target system, and the ideal homotopy would be one whose start system is sufficiently generic so that the degeneration of the start system to any target system would be possible [33]. However, the most generic start system can often increase the computational cost of the tracking, requiring to track many more solutions than the minimum number required. For a specific class of problems, then, introducing a specific and tailored start system can improve the performance of the algorithm.

Total degree homotopy

The first type of homotopy presented is a classical. Let d_i be the degree of the i-th polynomial in the system. In the *total degree homotopy* the start system is defined as:

$$\mathcal{G} = \begin{pmatrix} x_1^{d_1} - 1 \\ ... \\ x_n^{d_n} - 1 \end{pmatrix} \tag{6.3}$$

According to Bézout theorem (see [30], Chap. 18), the number of solutions of such a system is $N = \prod_{i=1}^{n} d_i$, and these solutions are given by:

$$x_i = e^{2\pi jk/d_i}, \qquad k = 1, ..., d_i, \quad \forall j \in [1, n] \tag{6.4}$$

where j is the imaginary unit.

Even if this start system is sufficiently generic to be applicable to different types of target system, and even if its solutions are simple to determine, the actual number of solutions that we need to track is in often smaller [34]. In fact, *N* is the maximum number of solutions that our target system can have, since we have built the most generic start system using the maximum degree of each polynomial in the target system. Assume that the total number of solutions of the target system is known, and let $M \leq N$ be that number. If we track all the *N* solutions of the total degree start system, we will end with $N - M$ *diverging* paths, which cannot be identified a priori and are computationally expensive to track. For this reason, it is sometimes desirable to use a different type of homotopy, with a more convenient start system, which has the same number of solutions as the target system. A way to compute the number M is to use techniques based on Gröbner bases [35].

Parameter homotopy

A type of homotopy that allows to track the optimal number of paths, equal to the number M of solutions of the target system $\mathcal{F}$, is the parameter homotopy. The idea is to build a start system which has the exact same structure of the target system, but depends on different parameters chosen randomly in the space of complex numbers. In fact, we can describe a polynomial system in terms of its variables (contained in $\mathbf{x}$) and its coefficient (depending on a set of parameters contained in $\mathbf{P}$). Making explicit this dependency and specializing $\mathbf{P} = \mathbf{P}_1$ for the target system, we can write $\mathcal{F} = \mathcal{F}(\mathbf{x}; \mathbf{P}_1)$. The start system can be defined as composed of the same equations of the target system, yet depending on different coefficients, so different parameters $\mathbf{P}_0$:

$$\mathcal{G} = \mathcal{F}(\mathbf{x}; \mathbf{P}_0) \tag{6.5}$$

The new system $\mathcal{H}$ of Equation 6.1 can be re-written as

$$\mathcal{H}(\mathbf{x}; \mathbf{P}, t) = \mathcal{F}(\mathbf{x}, t\mathbf{P}_1 + (1-t)\mathbf{P}_0) \tag{6.6}$$

If the parameters of the start and target system are *sufficiently generic*, so singular configurations are discarded, we can state that the parameter homotopy is globally convergent with probability one [22]. Since the two systems have the same structure and only differ for their coefficients, they will have the same number of solutions. A random choice of the parameters $\mathbf{P}_0$ makes the start system and its solutions general enough to be reusable for every other problem of the same family, until the parameters of the target system are sufficiently generic as well. When the start system has been solved once for all, the solutions of any other problem can be found tracking a number of paths exactly equal to the number of solutions of the target system.

The solutions of the start system can be obtained using an approach based on mon-

odromy. This method allows to determine the complex solutions of the initial set tracking a number of paths that is linear in the number of solutions, with small coefficient [33].

6.1.2 Homotopy applied to the IOD problem

The IOD polynomial system has been solved using the parameter homotopy of Equation 6.6, where the parameters are the entries of the $\mathbf{A}_i$ matrices encoding the observations. The start parameters are reported in Appendix B. The number of solutions of this system in terms of solution sets composed of $\{\mathbf{w}, \mathbf{g}, b\}$ is 66. This number is obtained removing all the solutions that are equivalent under sign symmetries that would leave the disk quadric invariant. The majority of these 66 solutions are complex, but they cannot be discarded a priori since, in the presence of noise, the right solution may fall in the complex space. The identification of the right orbit solution can be done with some practical considerations, both general and specific for the orbit considered, if some information is available. First, the pericenter of the recovered orbit must be higher than the orbited planet's radius. Also, the intersection between the estimated orbit and the LOS must occur in the direction of the observation, and not in the opposite direction. Another general requirement is that the LOS must not intersect the planet before meeting the orbit. This condition coincides with the previous requirement only when the observer is on the surface of the orbited body. Other considerations can be specific for the case but it is not guaranteed that all these conditions will remove all the realistic, non true solutions. The most simple way to solve the problem is to introduce an additional observation, if available, and check the norm of the residuals of the system when evaluated at this new observation.

CHAPTER 7

NUMERICAL RESULTS FOR BEARINGS-ONLY OBSERVATIONS

The homotopy-based solution has been applied to multiple scenarios of observation to study its performance under different geometries of the problem. First, it has been tested on an highly elliptical orbit, under well-spaced observations, to show the feasibility of the approach. Then, with the objective of understanding how nearly circular orbits were handled by the solver, a Low Earth Orbit (LEO) has been used with varying eccentricity, still keeping well-spaced observations so that the exclusive contribution of the eccentricity could be separated by other possibly challenging factors. This is of interest because of the decreased accuracy shown by the solver for the nearly circular orbit of the satellite AQUA [36] tested in [22] with respect to the highly elliptical orbit case. After that, the case of close observations has been analyzed to understand the sensitivity of the solver to the spacing between observations. This has been done both for the highly elliptical and the LEO, to gain different insights. Finally, the solver has been tested for observations gathered from observers in space.

The results provided by the method have been compared with those given by an implementation of the Double-R method. The implementation of the homotopy solver for lines of sight has been done in the software for algebraic geometry computation Macaulay2 [37] using the package NAG4M2 by Dr. Duff, one of the authors of the paper of reference of this work [22]. In all the simulations, the right solution was extracted among the others choosing the one with the smallest distance from the true, known, disk quadric. In this process, complex solutions have not been discarded since, with the addition of noise, the closest solution could be in the complex space.

Before moving to the analysis of the results, it is important to address the choice of the noise model. Considering exact knowledge of the position of the observer, the bearings

directions are modified in the following way: if $\mathbf{u}$ is the true direction of the satellite, the measured $\tilde{\mathbf{u}}$ is on the surface of a cone with vertex at the observer location, axis along the true direction and opening drawn from a normal distribution with 0 mean and standard deviation of σ. Given $\mathbf{u}$:

$$\tilde{\mathbf{u}} = \mathbf{u} + \boldsymbol{\epsilon} \tag{7.1}$$

where $\boldsymbol{\epsilon} \sim \mathcal{N}(\mathbf{0}, \mathbf{R})$ and $\mathbf{R}$ is the 3×3 matrix defined by:

$$\mathbf{R} = E[\boldsymbol{\epsilon}\boldsymbol{\epsilon}^T] = \sigma^2(\mathbf{I} - \mathbf{u}\mathbf{u}^T) \tag{7.2}$$

The matrix $\mathbf{R}$ has rank 2 and a null space in the direction of the true direction. This makes $\boldsymbol{\epsilon}$ lie in the plane normal to $\mathbf{u}$ and, if it is small, then we can still consider $\|\tilde{\mathbf{u}}\| = 1$ to the first order. The resulting measured direction lies on the surface of a cone with axis the true direction and opening sampled from a Gaussian distribution with norm 0 and covariance σ. This noise model is known with the name of QUEST Measurement Model (QMM)[38][39] and can be used to account for errors in the pointing accuracy. It has been used to perform a Monte Carlo simulation for each case analyzed.

7.1 Highly elliptical orbit: noiseless measurements

The first orbit analyzed is that of one of the spacecrafts of the Magnetospheric Multiscale mission (MMS) [40], assuming ideal observations gathered from three ground stations. The geometry of the problem is represented in Figure 7.1 and the orbital elements of the spacecraft are reported in Table 7.1.

Using five measurements, as required by the problem formulation, $N = \binom{10}{5} = 252$ possible combinations of five observations can be considered. The histograms in Figure 7.2

Table 7.1: Orbital elements of the MMS

a	e	i	Ω	ω
83519.02 km	0.9082	28.50°	357.84°	298.22°

show the errors in the estimation of the disk quadric and the orbital elements for all the 252 sets of observations. It is clear that the method can be used to recovery the orbit accurately, with errors in the estimation of the disk quadric (L2-norm), of the order of 10^{-13}. Now that the feasibility of the approach has been shown some other challenging geometries of observations will be tested.

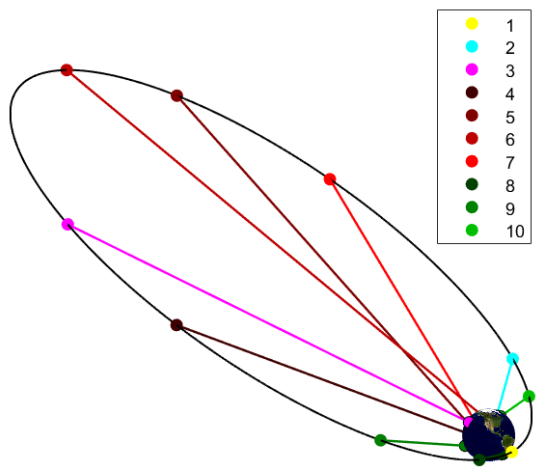

Figure 7.1: The MMS orbit and ten well-spaced observations.

7.2 Highly elliptical orbit: noisy measurements

The performance of the purely geometric approach has been tested and compared for several combinations of the 252 available from the noiseless analysis with that given by Double-R. Using the QMM noise model, a Monte Carlo simulation has been made for each of the configurations analyzed, using a noise level σ of 1 arcmin. The same perturbed inputs have been given to both the homotopy and the Double-R solvers, and the errors have been compared in terms of the estimation of the disk quadric and of the orbital elements. The Double-R method has been initialized using 3/4 of the true values of the radii of the position vectors; if, for some observations, this value was lower than the Earth's radius, the sum of the Earth's radius and 1/4 of the true slant range has been used as initial guess. For each group of five LOS used in the approach described in this work, however, there are ten

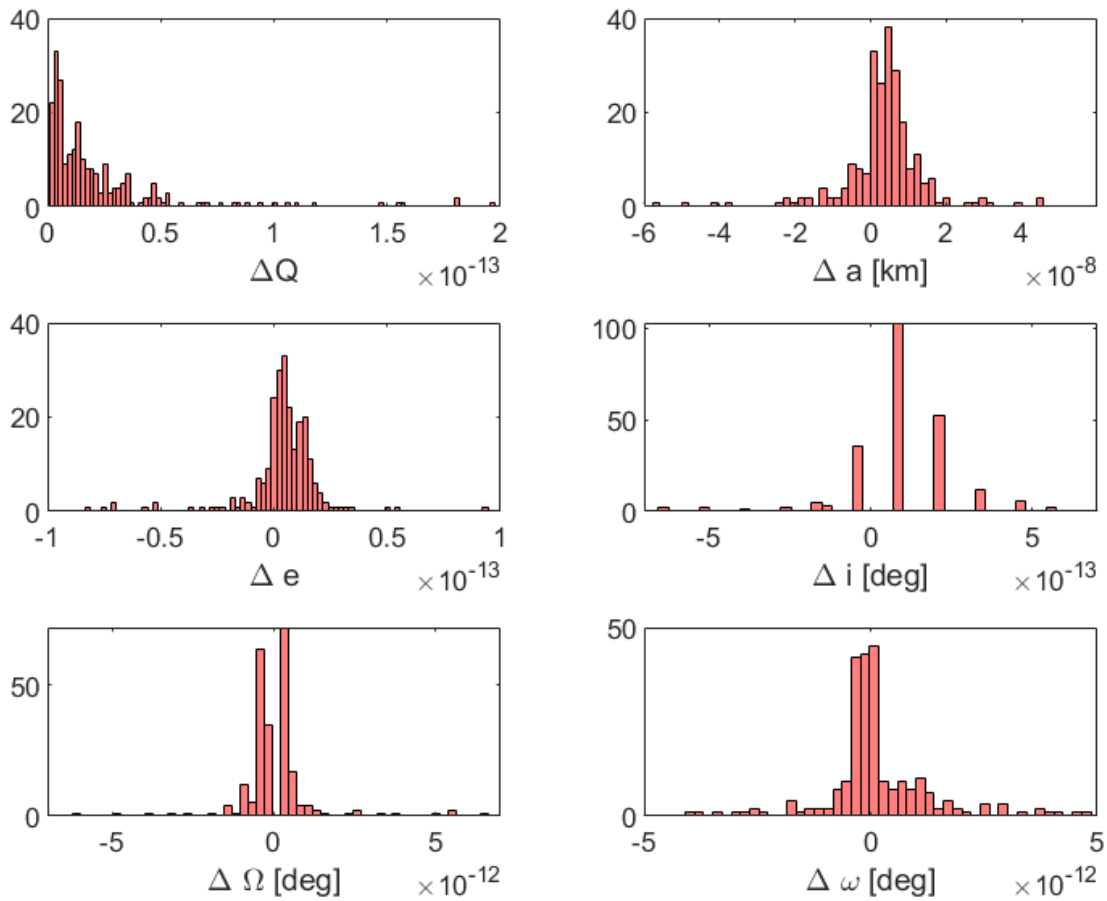

Figure 7.2: Errors in the estimation of the MMS orbit, ideal measurements, for 252 geometries of observation analyzed.

possible combinations of LOS that can be used as inputs of the Double-R method, since it only needs three LOS to work (and, of course, the knowledge of the time). For this reason, a comment on the general behavior over all the ten combinations should also be made.

The analysis of the results showed that the homotopy solution had a fairly stable accuracy independent of the combination of five observations chosen, while the Double-R showed a diversified range of behaviors. Making a fair comparison is not easy. On one hand, we are assuming that all the five observations are available, so we should consider the best solution provided by Double-R when comparing the performances of the methods. On the other hand, we are assuming that at least not all the time instants of the observations are known. In the ten combinations analyzed, however, the Double-R did not provide any

realistic result in four cases, and in the rest of the cases its performance, when compared in terms of the disk quadric, was always similar (slightly worse, except for one case where it was slightly better) to that of the homotopy solver. However, the disk quadric does not give all the details. In fact, the comparison between the accuracy in the estimation of each orbital element encloses more information. In most of the cases, the performance was similar to that shown on the left of Figure 7.3, where the two methods are competitive under 1 arcmin of noise in the measurements. However, in a couple of scenarios the aspect of the plots was different, with the Double-R estimating the in-plane features of the orbit (especially the semi-major axis) much more accurately than the homotopy solver (see Figure 7.3, right-hand side). This pattern will be met again in the next simulations, where in the most challenging conditions of observation the homotopy solver will estimate more reasonably the orbital plane than the size and shape of the ellipse in that plane.

The overall conclusion drawn from this first analysis and similar analyses made on the whole set of 10 observations is that for well-spaced observations the two methods have

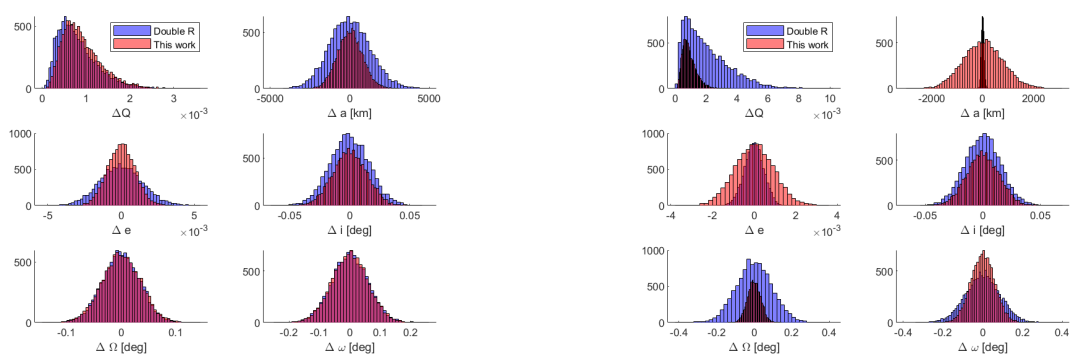

Figure 7.3: The homotopy-based solution is competitive with one of the state of the art algorithms for IOD. Even if Double-R struggled to converge for most of the configurations analyzed, it was sometimes better in the estimation of the in-plane parameters. On the other hand, the homotopy-based solution was usually more accurate in the estimation of the orbital plane. Note how the maximum relative error in the estimation of the semi-major axis is less than 2.5% for the homotopy solution. The left and right plot differ in the three observations, extracted from the five available, used to implement Double-R. Results obtained under $\sigma = 1$ arcmin, for 10000 runs.

.

similar performance, with Double-R showing a more variable behavior and sometimes failing the run, and the homotopy solver behaving consistently as the set of observations used changed. Also, it should be noticed that the Double-R needed an initialization and used perfect values of the instants of observation. On the other hand we recall that the homotopy solver was able to produce these results without any use of time-of-flight measurements and without any initial guess of the orbit. This proves that the homotopy solver is a competitive tool for the estimation of highly elliptical orbits, for well-spaced observations.

7.3 Nearly circular orbits: noisy observations

In this section, a LEO has been considered and its eccentricity has been gradually decreased, keeping fixed all the other orbital elements, to study how nearly circular orbits are handled by the algorithm. This case is of interest since for a circular orbit the eccentricity is equal to zero, then $c = 0$ and $\mathbf{g} = \mathbf{0}$ is no more an unknown of the problem, so $n = 3$ observation should in theory be sufficient to recover the orbit. Introducing this information *a priori* would make the system with five observations over-determined. This approach was followed in [22], with the introduction of a *circular model* as opposed to the *elliptical model* used until now. When the circular model was used, a bias was introduced in the results, but this increased the accuracy of the solution, making it comparable with the performance of Double-R. This created the interest in understanding whether nearly circular orbits were a problematic case for the solver.

The orbital elements of the orbits used are shown in Table 7.2, where the only varying one is the eccentricity.

Table 7.2: Orbital elements for the LEO.

a	e	i	Ω	ω
9000 km	$10^{-1,-2,-3,-4}$	30.00°	126.232°	66.231°

The results obtained in the ideal case are reported in Table 7.3 and the configuration of observation is represented in Figure 7.4 for the orbit with $e = 10^{-3}$. Note that the latitude

of the pericenter ω is undefined for circular orbit, so its estimate is not of importance and will be omitted.

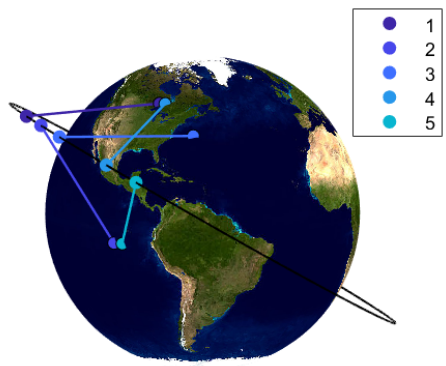

Figure 7.4: Observations for the nearly-circular orbit, three ground stations.

Table 7.3: Errors in the estimation of the orbital elements as the orbit is deformed into circular, ideal measurements. The four cases correspond to the four values of eccentricity used. The measurements used have been taken at the same instants for each of the four cases.

orbit	$\Delta\|Q\|$	$\Delta a[km]$	Δe	$\Delta i[deg]$	$\Delta\Omega[deg]$	$\Delta\omega[deg]$
$e = 10^{-1}$	$7.83\,10^{-15}$	$6.00\,10^{-11}$	$3.72\,10^{-15}$	$7.00\,10^{-14}$	$7.63\,10^{-14}$	$2.68\,10^{-12}$
$e = 10^{-2}$	$6.06\,10^{-14}$	$-7.09\,10^{-11}$	$-1.72\,10^{-15}$	$7.00\,10^{-14}$	$< 10^{-16}$	$-3.43\,10^{-11}$
$e = 10^{-3}$	$1.41\,10^{-12}$	$2.24\,10^{-10}$	$1.70\,10^{-14}$	$-4.45\,10^{-14}$	$1.27\,10^{-13}$	$1.07\,10^{-9}$
$e = 10^{-4}$	$1.00\,10^{-4}$	$-3.64\,10^{-12}$	$-1.00\,10^{-4}$	$-4.45\,10^{-14}$	$5.09\,10^{-14}$	13.47

The method shows a quite robust behavior under 1 arcmin of noise in the observations. In Figure 7.5 the errors in the estimation of the orbital elements are represented. For comparison, the Double-R has been tested over the same noisy data sets. Only in three of the 40 cases analyzed (combinations of three observations taken from five, for each of the four orbits), the Double-R method was able to converge, with an initial guess for the radii equal to 3/4 of the true values. In those three cases, the performance was comparable with that of the homotopy solution, showing a slightly better estimation of the in-plane parameters, with the homotopy being better at estimating the orbital plane attitude and orientation. Also in this scenario, the homotopy-based solution showed to be competitive with one of the state of the art algorithms for IOD. In particular, it was much more reliable in actually finding a

solution.

This may seem to contrast with the results obtained in [22], where the testing of the method over a nearly circular orbit produced results that, in comparison with those produced by the solver when the orbit was constrained to be circular, were poorer. However, the results reported in that work were obtained, even if that was not explicitly written, for a configuration of observations which was not far from the singular condition of coplanar observations. This addresses the problem presented in [22] about the choice of which model (elliptical or circular) should be chosen to approach the IOD.

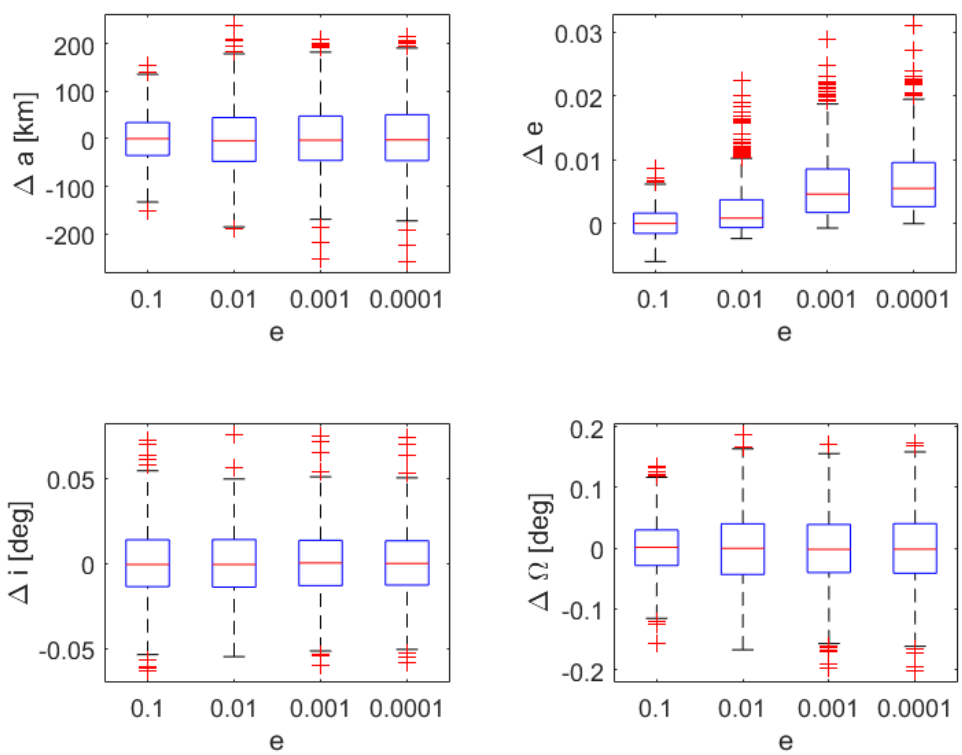

Figure 7.5: Errors in the estimation of the orbital elements for decreasing eccentricity of the LEO. Note that the errors remain reasonable as the eccentricity decreases. The red line represents the median value. The blue box encloses the 50% of the results while the two black markers delimit the minimum and the maximum values. Each red marker '+' represents a value considered as an outlier.

7.4 Close observations

The following objective was to understand the performance of the algorithm when close observations are used. This has been done both for the MMS and the LEO with $e = 0.1$. The reason why two orbits have been analyzed is that the high eccentricity of the MMS makes the observed points almost collinear in the 3D space and the lines of sight almost coplanar. For this reason, observations made in correspondence of arcs of orbit with higher curvature and closer to the observer were desired to decouple the almost coplanarity of the observations from the closeness of the observed positions along the orbit. Since 1 arcmin of noise led to completely unreliable results, especially in the estimation of in-plane features of the orbit, the study has been performed for increasing levels of noise: between 0.1 arcsec and 10 arcsec, values compatible with the instrumentation available nowadays. Starting from the MMS, the geometry of the observations, which are gathered by three ground stations, is represented in Figure 7.6. Note that the total angular separation of the observed positions was of roughly 7.5 deg in true anomaly.

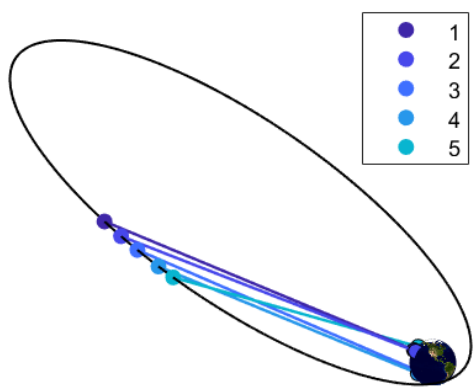

Figure 7.6: Close observations for the MMS from three ground stations.

The results obtained from a Monte Carlo simulation with 1000 runs are reported in Figure 7.7 for each level of noise. Note how the performance starts to degrade quickly as the noise increases above 1 arcsec, especially in the estimate of the semi-major axis.

Interestingly, Double-R was not able to converge even for 0.1 arcsec of noise, for any

of the ten combinations of observations, when initialized with 3/4 of the true values for the radii. For this reason, the results have been compared with those provided by an implementation of Gauss' method as described in [18]. Also in this case, there are 10 possible combinations of observations that can be tested. As for Double-R in the previous analysis, the performance of Gauss was variable depending on the observations provided. In all the

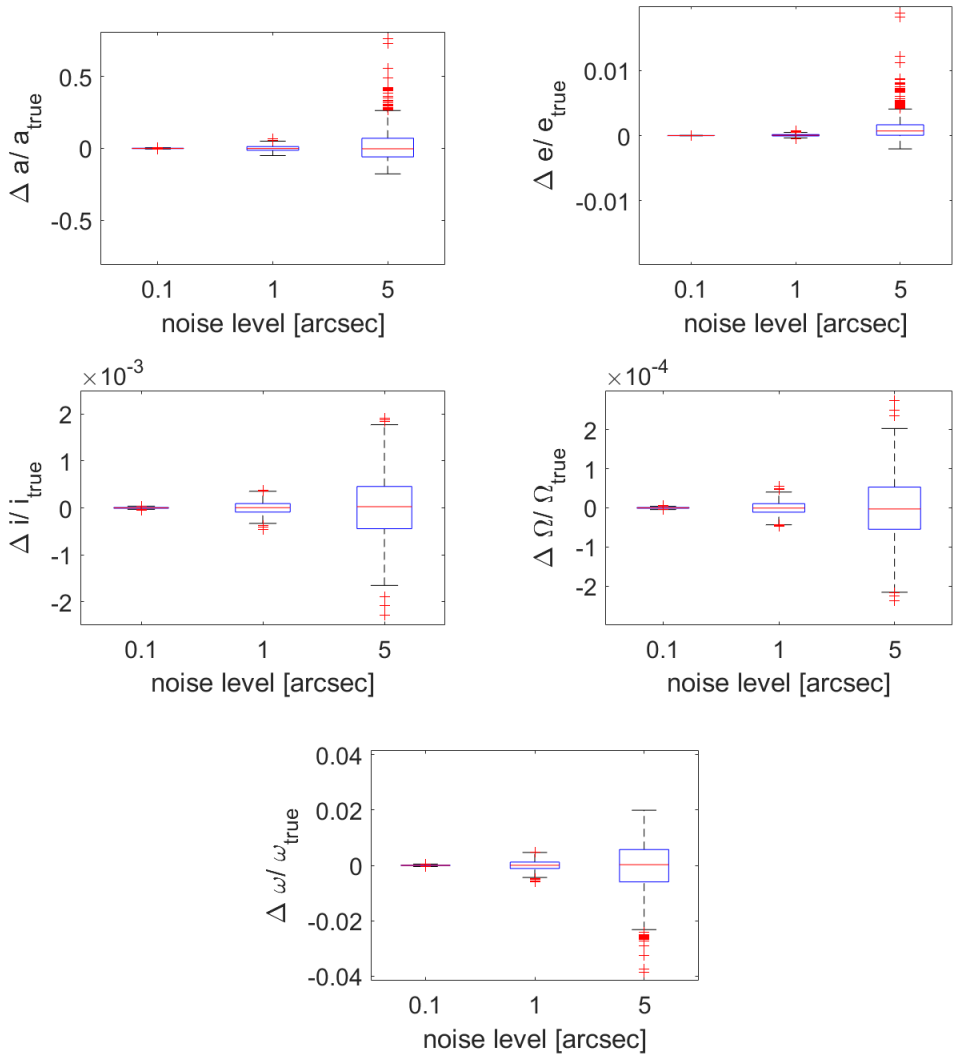

Figure 7.7: Errors in the estimation of the orbital elements for increasing noise, highly elliptical orbit, close observations. Note how the performance degrades quickly as the noise increases, especially in the estimate of the in-plane parameters.

cases, except for one, the results showed a bias, and the biggest errors were in the estimate of the semi-major axis, while the other parameters were estimated accurately. The best solution provided by Gauss for 1 arcsec of noise is compared with the solution obtained with the homotopy-based approach in Figure 7.8. As we can see, in general Gauss behaved better, being more accurate in the estimate of most of the parameters.

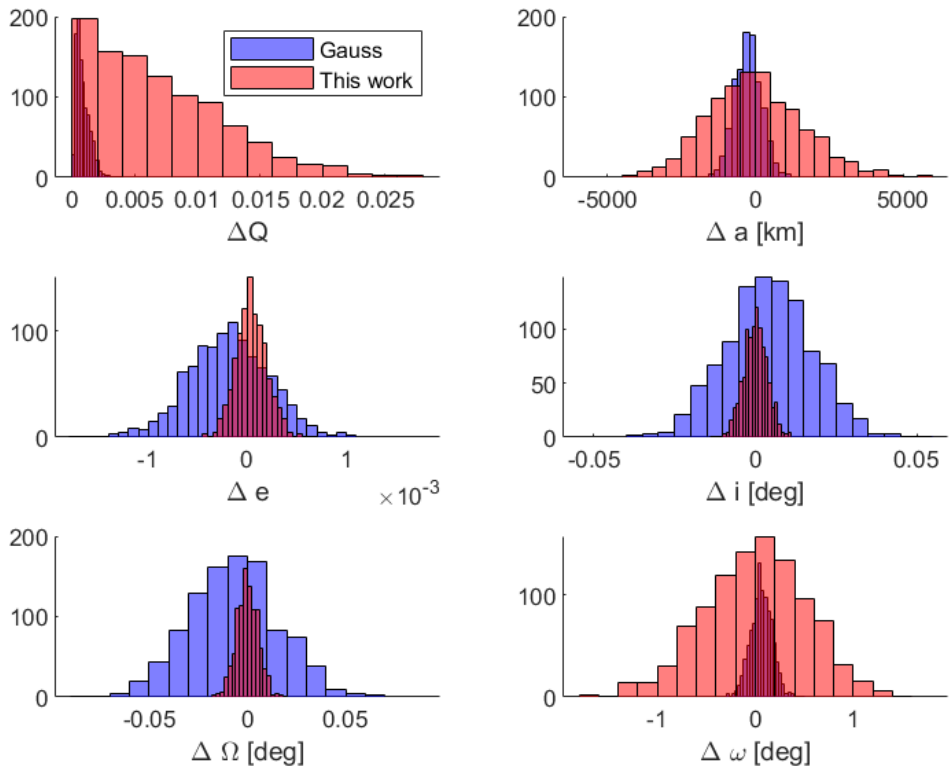

Figure 7.8: Errors in the estimation of the orbit for the MMS, 1 arcsec of noise, close observations, compared with the results provided by Gauss. Note that the maximum relative error in the estimate of the semi-major axis is of 6% for the homotopy solution. The method can handle much less noise when the observations are close, especially if they are almost coplanar.

After that, close observations on a LEO have been analyzed to understand whether the almost coplanarity of the observations for the MMS was the cause of the lower tolerance to the noise. The geometry of the observation is represented in Figure 7.9, where the angular separation between the two extreme positions along the orbit is of about 9.8 deg in true

anomaly. Note that the observed positions are much closer than in the MMS case because their distance from the focus of the conic is smaller.

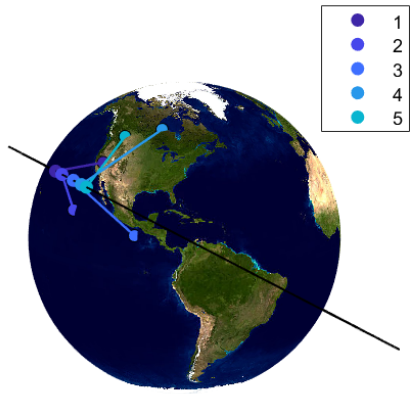

Figure 7.9: Geometry of the IOD problem for close observations on a LEO.

Differently from above, the observations are not gathered from three ground stations but from five, to guarantee more diversity in the geometry. This increased the accuracy of the results, as shown in Figure 7.10, where we can see that the method can handle an higher amount of noise. Nonetheless, this amount of noise is definitely lower than that used in the case of well-spaced observations, suggesting that having close observations is an unfavorable condition for this method for levels of noise which are too high. Note that the Double-R method, tested over the same inputs, was never able to converge, for 1 arcsec of noise, when initialized with 4/5 of the true vales. Even when the initialization was made with the true values, 1 arcsec of noise was enough to make half of the runs fail. On the other hand, the performance of the best solution obtained with Gauss was better. This is shown in Figure 7.11 for 1 arcsec of noise, suggesting that for close observations, if time information is available, Gauss method should probably be the first choice.

7.5 Observations from space

Since no assumption is made on the position in space of the LOS, this method should in theory continue to provide reasonable results even in case of observers in space. For this

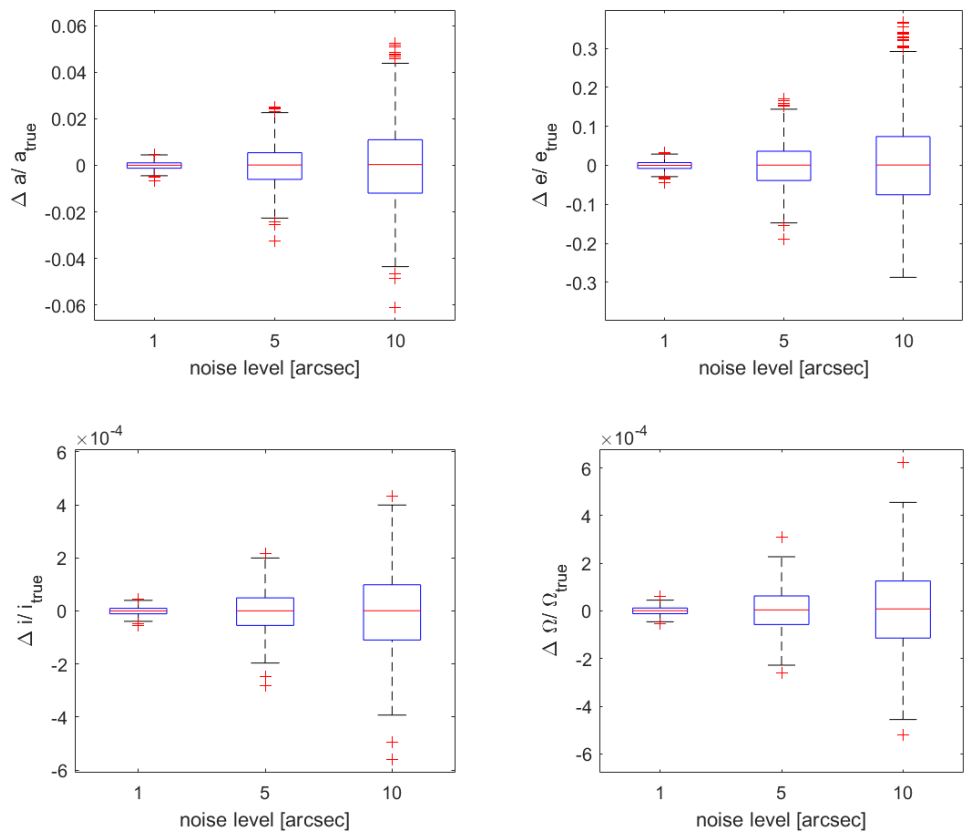

Figure 7.10: Errors in the estimation of the LEO, close observations. Note how the performance starts to decrease for values of noise higher than those that limited the accuracy in the estimate of the MMS orbit. Again, the parameters that degrade first are the in-plane ones.

reason, the estimation of the LEO has also been attempted for a single observer orbiting in Geosynchronous Equatorial Orbit (GEO). In the noiseless analysis, the solver was able to estimate the orbit with an error of the order of 10^{-13} in the disk quadric.

When noise is introduced in the bearing measurements, however, the LOS perfectly pass through the GEO and do not exactly intersect the LEO. In this case, the estimator tended to lock into the estimation of the observer's orbit. Among the 66 solutions obtained for a run made with 1 arcmin of noise, the solver produced an estimate of the GEO as precise as reported in Table 7.4. The other solutions produced disk quadrics that were not

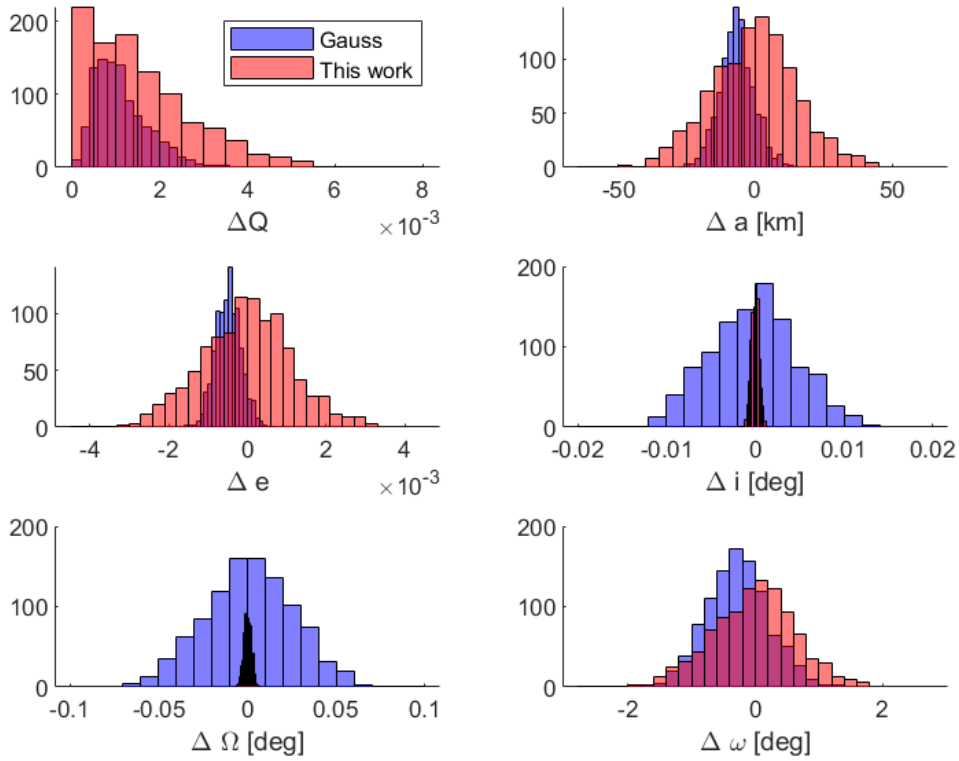

Figure 7.11: Errors in the estimation of the LEO for close observations and 1 arcsec of noise compared with the results provided by Gauss method. Under this geometry, where more diversity in the inclination of the LOS was provided, the homotopy approach could handle more noise than in the previous case, but it is again outperformed by the solution obtained with Gauss.

close to the spacecraft's orbit. However, this result is useful because it shows again that the estimation of perfectly circular orbits is possible with the solver, and that the elements of **g** can go to zero independently exploiting the information enclosed in the five measurements.

It has been also noticed that the main reason of the absence of the true solution orbit among the others is the almost coplanarity of the observations. Since the radius of the GEO was almost 5 times the radius of the LEO, the diversity in the inclination of the LOS was not appreciable. If the observations are gathered from different orbits, or if they are gathered from a single orbit with smaller radius (which guarantees the departure from the coplanarity condition in this case), finding a solution becomes again possible, as shown in

Figure 7.12 for three observers in three circular orbits at different inclinations. Since the Double-R method is based on the assumption that the observer's distance from the focus is smaller than the satellite's distance, so it cannot be used, the results have been compared with Gauss' method. The homotopy solution proved to be by far more accurate than the Gauss'. A comparison between the error in the estimation of the disk quadric is given in Figure 7.13.

Table 7.4: Comparison between the estimated, the true and the observer's orbital parameters for a single observer in GEO

	w_1	w_2	w_3	g_1	g_2	g_3	b
Searched orbit	0.4033	0.2955	0.8660	-0.0628	-0.0103	0.0328	8954.89
Observer's orbit	0	0	1	0	0	0	42164
Estimated orbit	2.0210^{-14}	-1.1410^{-13}	1	0.1510^{-11}	0.0210^{-11}	0	42164.00

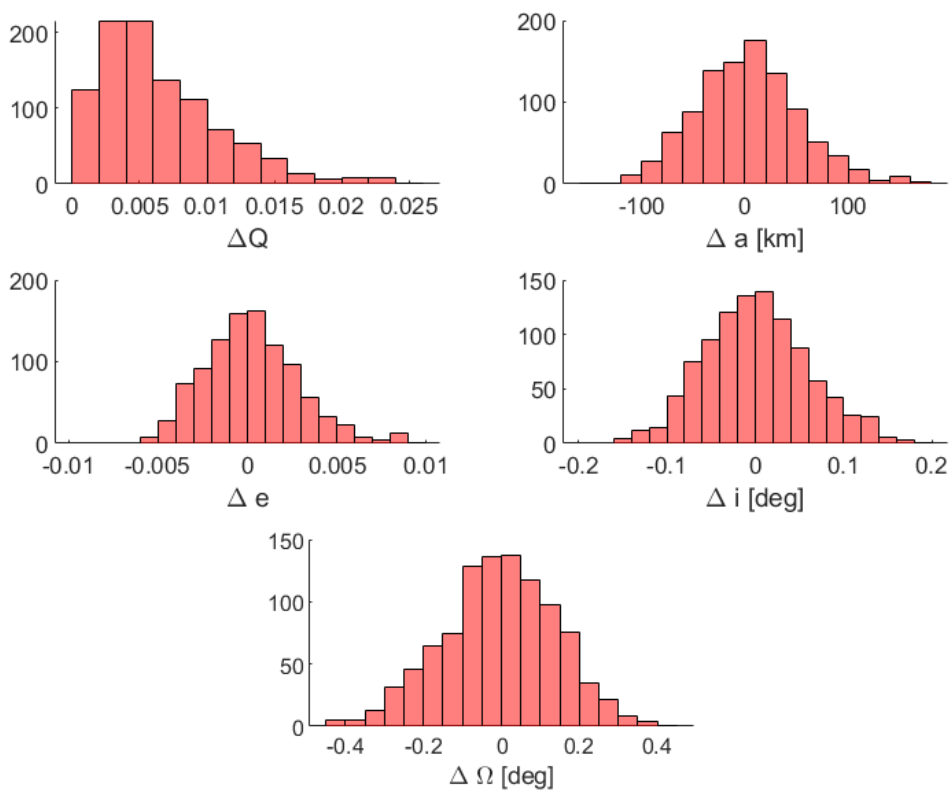

Figure 7.12: Errors in the estimation of the LEO for observations made from space, 1 arcmin of noise.

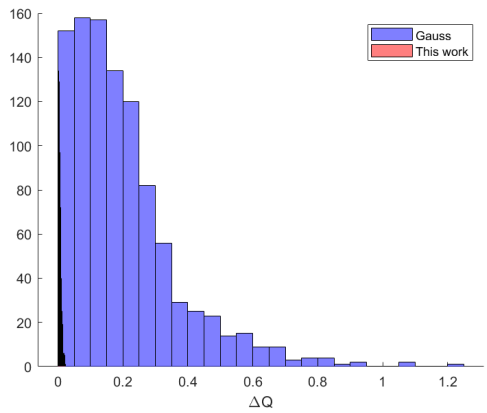

Figure 7.13: The results obtained with Gauss' method are much less accurate than those obtained with the homotopy solution for 1 arcmin of noise. Note that the same perturbed inputs have been used for the two solvers.

CHAPTER 8

EXPERIMENTS WITH STREAKS AND LINES OF SIGHT

In this chapter, the performance of the homotopy solver when streaks and LOS are used is analyzed. This simulation had the main objective of understanding whether the introduction of streaks could improve the performance of the solver, especially where it was more defective. Recalling what has been derived in chapter 5, two different types of constraints can be imposed on streak observations, both linear in the entries of $\mathbf{Q}^*$, depending on the assumptions made. Recalling that n_{LOS} is the number of LOS observations, n_{PP} is the number of streaks over which the point-to-point constraint has been imposed and n_{LP} is the number of line-to-plane constraints, we can freely choose these numbers until

$$n_{LOS} + 2n_{PP} + n_{LP} = 5 \tag{8.1}$$

Clearly, the use of point-to-point constraints reduces the number of measurements necessary to solve the problem, with the smallest value obtained with one LOS observation and two point-to-point constraints. For the whole analysis, the observers are considered fixed in the inertial space. The exposure time has been varied depending on the satellite tracked [41]. For the LEO, an exposure time of 1 s has been used, while for the MMS orbit it was of about 8 s.

8.1 Noiseless results

In the noiseless case, the streaks have been simulated finding the best-fit line through the points imaged by a camera when observing the position of the satellite for the exposure time. This process already introduces an error in the algorithm, even for ideal bearing measurements, since the arc of trajectory projected on the image is in theory elliptical and

is approximated through a line. However, the observed accuracy in the estimation of the disk quadric is of the order of 10^{-9} or less for all the combinations of constraints, so the observation duration is small enough to make the linear approximation reasonable.

8.2 Noisy results

The noise model used for the LOS was the same used above, with 1 arcsec of standard deviation. For the streaks, the noise has been sampled from a Gaussian distribution with zero mean and covariance matrix $\mathbf{R} = diag(tan(\sigma^2/3))$ where, again, $\sigma = 1$ arcsec. This noise has been applied to the endpoints of the streak, producing altogether a rotation, a stretching, and a translation. The results obtained for the LEO are shown in Figure 8.1. From the plots we can see that the use of the point-to-point constraint, i.e. the assumption that the streaks represents the projection of the velocity at the midpoint, is not acceptable in presence of noise, since it consistently lowers the accuracy and introduces a bias. This has been confirmed by the analysis of the minimum input configuration, which only requires one LOS and two streaks (over which the point-to-point constraints must be imposed). In this case, in fact, the errors obtained in the estimation of the disk quadric were of about the 80%. The use of streaks as simple projection of a tangent plane (line-to-plane constraint), instead, seems to be a valid replacement for LOS observations. This can be appreciated in Figure 8.2, where only line-to-plane constraints have been used.

The same experiment has been then repeated for the MMS orbit with close observations, as in the previous chapter. The introduction of any type of streak constraint make the solver's accuracy decrease greatly, converging to the wrong solution in almost all the cases. This suggests that the use of streaks is not a means to give robustness to the solver when the singular configuration is approached, but instead makes it more prone to failure.

Summarizing, the assumption that the streak is the projection of a line tangent to the orbit in the orbital plane seems to be acceptable, providing results which are almost comparable with those provided by LOS only observations, when we are far from the singularity

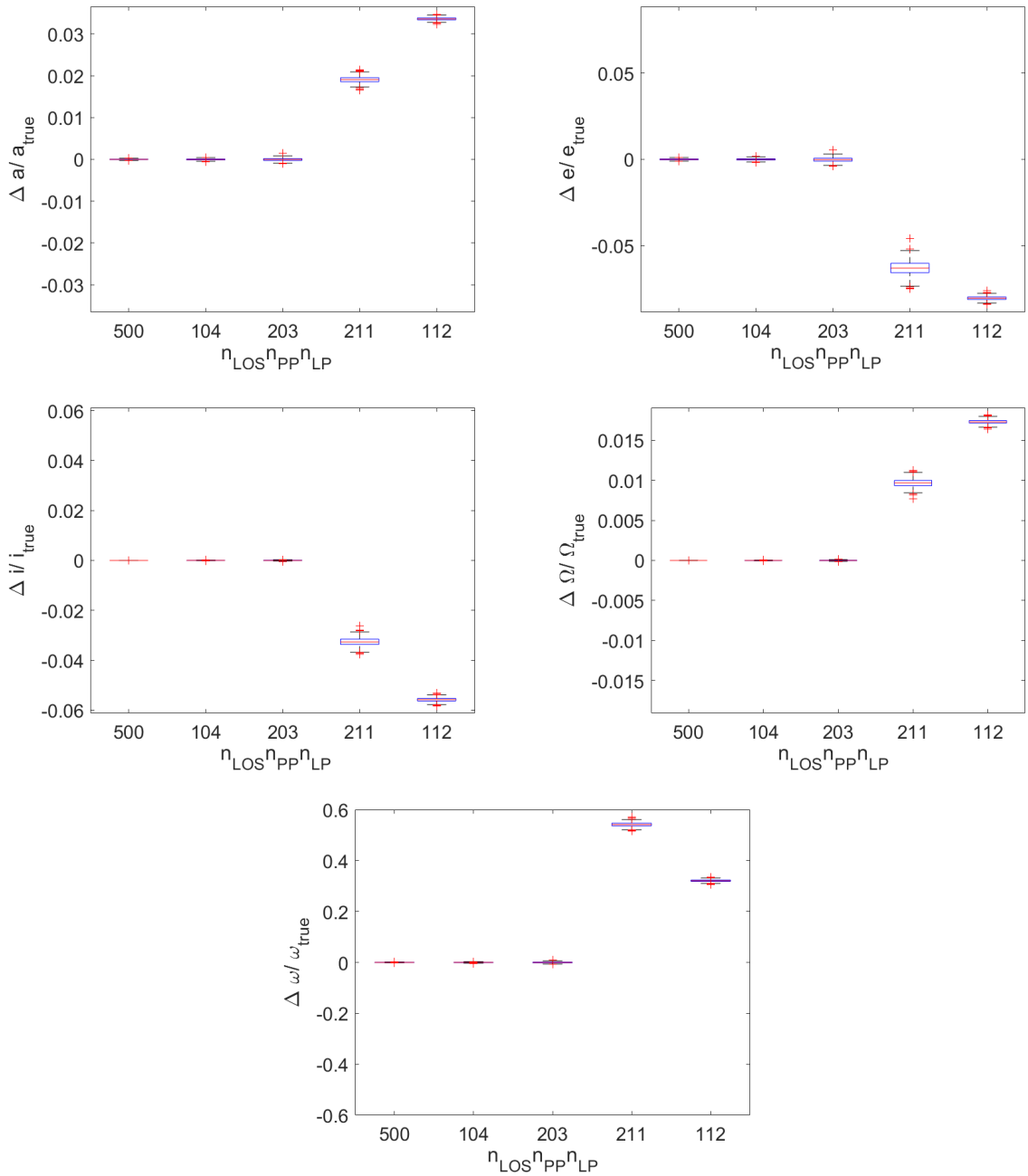

Figure 8.1: While the assumption that the streak is contained in a plane of the disk quadric provides reasonable results, introducing the assumption that the point of tangency of that plane projects to the the midpoint degrades the accuracy and introduces a bias. A zoom of the first three results can be found in Figure 8.2.

condition of almost coplanar observations. On the other hand, assuming that the point of tangency projects to the streak's midpoint introduces a bias and degrades the accuracy. It has been tested that the main source of the error in the point-to-point constraint is the rotation of the streak. In fact, translations of the streaks under 1 arcsec of noise produce data that are utilizable in the configuration with the minimum number of inputs, yet introducing a bias. Also, the introduction of streaks doesn't help in improving the accuracy where the solver was more defective, in the condition of almost coplanarity of close observations. Moreover, since the whole study has been performed with stationary observers, it is expected that in real conditions the performance will degrade, as happened in [3], since the streaks would be parallel to the relative velocity vector at some point of the orbit and not to the absolute velocity.

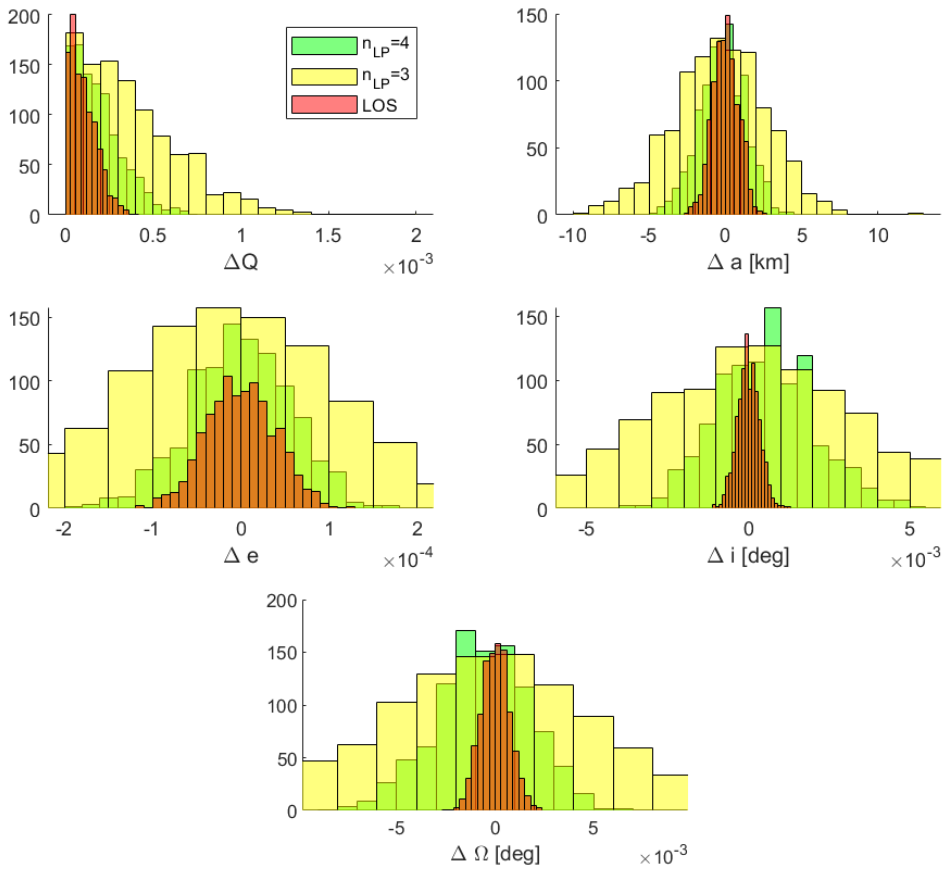

Figure 8.2: The assumption that the streaks and the observers define planes that are tangent to the orbit provides results that continue to be plausible, with the accuracy only slightly decreased by the presence of streaks.

CHAPTER 9
CONCLUSIONS AND FUTURE WORK

In this work, a purely geometric solution of the angles-only IOD problem has been analyzed. This solution, based on a reformulation of the Keplerian orbit as a disk quadric, produced a polynomial system that needs five line of sight observations to produce a finite number of solution orbits. Discerning the true solution among the others is possible when specific considerations are introduced. For example, associating a sign to the direction of observation (the satellite is along the LOS in front of the observer, and not behind), reduces the number of solutions, as well as discarding all those orbits with pericenter lower than the orbited planet's surface. Other orbits can be rejected if even a rough knowledge of the time of flight between the observations is known. Complex solutions cannot always be discarded a priori when noise is introduced, but in all the simulations made the solutions never fell into the complex space. Also considering all these elements, it is not guaranteed that a single solution orbit will remain. The more direct way is to use an additional observation and check the residuals of the system when evaluated for the new measurement.

The method was tested both on well-spaced and close observations, and its performance over challenging geometries of observation has been assessed. In the tests made, it proved to be competitive with one of the state of the art algorithms for IOD, the Double-R method. When well-spaced observations are used, the method showed fairly stable accuracy in the estimation of the orbit over varying combinations of observations, providing reasonable results even when the noise in the measurements had a standard deviation as high as 1 arcmin. The performance decreased when close observations were used, especially if they tended to be coplanar. However, the condition of coplanarity is a singularity condition common among the angles-only IOD problem, being intrinsic in the nature of the problem [42]. This problem is in fact encountered in the other classical solutions, among which

are Gauss and Laplace methods. Still, the homotopy-based approach was able to provide plausible results where the Double-R method failed completely, showing a more robust behavior in the unfavorable condition analyzed. When the LOS intersect more than one orbit, however, as in the case of a single observer in space, a nearly singular configuration of observations may lead to the locking of the algorithm into the estimation of the observer's orbit.

When the conditions of observation are not favorable, the homotopy-based solution showed to be more reliable in the estimation of the orbital plane than in the estimation of the in-plane parameters. This has been seen, for example, in the case of close and almost coplanar observations where, as the noise level increased, the estimate of the in-plane parameters degraded much more quickly. Unless the closeness to the singular configuration is extreme, then, the method can be a resource to provide an initial guess of the angular orbital elements, that could help in estimating some parameters for the initialization of other classical IOD solutions. It is also important to emphasize that the method suffered when using close observations in the test cases analyzed, providing results that were worse than those obtained with Gauss. Again, a diversity in the inclination of the LOS is a way to increase the accuracy of the solver. Note that Double-R failed to converge in these cases, while Gauss failed to converge in the previous cases analyzed of well-spaced observations. In summary, the homotopy-based solver behaved reasonably for well-spaced observations and could handle close observations for small amounts of noise (below 5-10 arcsec in the cases analyzed), continuing to provide a solution, especially when a departure from the singular configuration is guaranteed.

An additional comment should be made on the estimation of nearly circular orbit. In contrast with the initial analysis of the data obtained in [22], the nearly circular solution has not created particular problems in the test cases analyzed. In fact, even if three observations are sufficient to estimate the circular orbit when introducing the constraint $\mathbf{g} = \mathbf{0}$, if this constraint is not imposed a priori the elements of the vector $\mathbf{g}$ seem to go to zero

independently. This has been verified when a test has been made to estimate an orbit for observations gathered from a GEO. Since all the LOS intersected two possible orbits (the satellite's and the observer's), the solver provided the GEO among the other solutions, and that perfectly circular orbit was recovered without troubles. When the observations tend to be coplanar, and the estimated orbit is nearly circular, constraining a priori $\mathbf{g} = \mathbf{0}$, i.e. using the *circular model* of [22], is a resource that can improve the accuracy of the results, yet introducing a bias.

Other research in progress showed that the use of more than five observations can increase the accuracy of the solver, where the loss function minimized was the sum of the algebraic quantity on the left-hand side of Equation 4.6 evaluated for each observation. The analysis of this constraint made in this work led to the conclusion that the best-fit orbit obtained in this way is not necessarily the orbit that, once projected, best fits the points observed on the camera images. Other research is in progress to understand whether a polynomial constraint can be obtained to optimize the solution in that sense.

Probably, the main distinctive features of this approach are its inputs. The use of LOS, that can be obtained through simple cameras or telescopes, and the absence of time-of-flight information, reduce the complexity of the instrumentation devoted to the IOD task. First, there is no need to worry about clock synchronization necessary to collect, for example, one-way range information. Also, there is no need to collect the instant of the measurements and to make corrections for the light time-of-flight necessary in the estimation of the two-way range. The problem of the non-zero light time-of-flight, however, does not affect only the range estimation, but is something that must be taken into account even when LOS observations are used if time is considered a known parameter in the algorithm. Eliminating time from the process, this problem is solved and the pre-processing of the data is decreased. In fact, for this method to work, it is sufficient that the LOS intersect the orbit, and this happens even if we are observing a position occupied by the satellite in the past. The only step where time is needed is in the determination of the observer's position.

Another important characteristic is that the solver is global, in the sense that it doesn't need to be initialized. The homotopy-based solution, in fact, works without any type of initial guess. This makes it suitable for situations where the orbiting object is sighted for the first time.

Two other characteristics have been noticed in the comparison of the performance with the Double-R method. First, for the Double-R method to work in the case of retrograde orbits, the direction of motion must be inserted as input to the algorithm. If this is not done, it provides completely unreliable results. On the other hand, the homotopy solution worked without requiring such information as input. Finally, the Double-R method has among its assumptions that the distance of the satellite from the center of the orbited planet is greater than the observer's distance. This is usually true, when the observer is on the Earth's surface. However, when the observer is in space, this can cause issues. Since the homotopy-based solution does not make this type of assumptions, it is in theory more suitable for this type of applications. This has been tested for observers in circular orbits. As already discussed, using observations gathered from a single orbit will make the solver produce the observer's orbit among the others, with that orbit being the only one produced if the observations are almost coplanar. However, if the observations are gathered in such a way that the singularity is avoided, or are gathered from different orbits, the solver can be used to recover the right orbit. A general consideration that is valid for all the cases is that the more diverse are the LOS observations, the higher is the accuracy obtained.

In conclusion, the homotopy approach proved to be more reliable than the classical methods which have been used to make a comparison in actually providing a solution. On one hand, Gauss's method was not able to provide a reasonable solution when the observations were too far apart, as expected. On the contrary, the homotopy-based approach always provided a solution, with the exception of geometries extremely close to the singular configuration, where both the Gauss and Double-R method failed to converge too.

The partial substitution of LOS observations with streaks was also tested. The results

showed that the approximations introduced at the basis of the theory caused an error that is, in general, higher than that produced by bearings-only observations. The substitution of LOS with streaks is feasible in standard conditions of observation, while the results are not reliable in the case of almost coplanar data. Also, the most accurate description of the relationship between the streak and the disk quadric seems to be that the plane defined by the streak and the observer is tangent to the orbit, leaving the point of tangency being free to be anywhere. Constraining the midpoint to be the point of tangency, even though it reduces the number of inputs necessary to solve the problem, introduces a bias in the results and decreases the accuracy heavily.

Appendices

APPENDIX A

POLYNOMIAL CONSTRAINTS

The expansion of the three polynomial constraints proposed in chapter 4, after factorization and normalization, always led to the same polynomial, whose coefficients are expanded in the table below. Note that the polynomial is of degree three, as predicted from the analysis of subsection 4.2.1.

$g_2w_1^2$	$-2x_2u_3^4+2_2x_3u_3^3$
$g_3w_1^2$	$2x_3u_2^2u_3^2-2x_2u_2u_3^3$
$-\frac{1}{b^2}w_1^2$	$-u_2^2u_3^2x_3^2+2u_2u_3^3x_2x_3-u_3^4x_2^2$
w_1^2	$-u_2^2u_3^2-u_3^4$
$g_1w_1w_2$	$2x_2u_3^4-2u_2x_3u_3^3$
$g_2w_1w_2$	$2x_1u_3^4-2u_1x_3u_3^3$
$g_3w_1w_2$	$2u_1u_3^3x_2+2u_2u_3^3x_1-4u_1u_2u_3^2x_3$
$-\frac{1}{b^2}w_1w_2$	$2u_3^4x_1x_2-2u_1u_3^3x_2x_3-2u_2u_3^3x_1x_3+2u_1u_2u_3^2x_3^2$
w_1w_2	$2u_1u_2u_3^2$
$g_1w_1w_3$	$-2x_3u_2^2u_3^2+2x_2u_2u_3^3$
$g_2w_1w_3$	$2u_2u_3^3x_1-4u_1u_3^3x_2+2u_1u_2u_3^2x_3$
$g_3w_1w_3$	$2x_1u_2^2u_3^2-2u_1x_2u_2u_3^2$
$-\frac{1}{b^2}w_1w_3$	$-2x_1x_3u_2^2u_3^2+2x_1u_2u_3^3x_2+2u_1x_3u_2u_3^2x_2-2u_1u_3^3x_2^2$
w_1w_3	$-2u_1u_3^3$
$g_1w_2^2$	$-2x_1u_3^4+2u_1x_3u_3^3$
$g_3w_2^2$	$2x_3u_1^2u_3^2-2x_1u_1u_3^3$
$-\frac{1}{b^2}w_2^2$	$-u_1^2u_3^2x_3^2+2u_1u_3^3x_1x_3-u_3^4x_1^2$
w_2^2	$-u_1^2u_3^2-u_3^4$
$g_1w_2w_3$	$2u_1u_3^3x_2-4u_2u_3^3x_1+2u_1u_2u_3^2x_3$
$g_2w_2w_3$	$-2x_3u_1^2u_3^2+2x_1u_1u_3^3$
$g_3w_2w_3$	$2x_2u_1^2u_3^2-2u_2x_1u_1u_3^2$
$-\frac{1}{b^2}w_2w_3$	$-2x_2x_3u_1^2u_3^2+2x_2u_1u_3^3x_1+2u_2x_3u_1u_3^2x_1-2u_2u_3^3x_1^2$
w_2w_3	$-2u_2u_3^3$
$g_1w_3^2$	$-2x_1u_2^2u_3^2+2u_1x_2u_2u_3^2$
$g_2w_3^2$	$-2x_2u_1^2u_3^2+2u_2x_1u_1u_3^2$
$-\frac{1}{b^2}w_3^2$	$-u_1^2u_3^2x_2^2+2u_1u_2u_3^2x_1x_2-u_2^2u_3^2x_1^2$
w_3^2	$-u_1^2u_3^2-u_2^2u_3^2$
g_1^2	$-u_2^2u_3^2x_3^2+2u_2u_3^3x_2x_3-u_3^4x_2^2$
g_1g_2	$2u_3^4x_1x_2-2u_1u_3^3x_2x_3-2u_2u_3^3x_1x_3+2u_1u_2u_3^2x_3^2$
g_1g_3	$-2x_1x_3u_2^2u_3^2+2x_1u_2u_3^3x_2+2u_1x_3u_2u_3^2x_2-2u_1u_3^3x_2^2$
g_1	$2x_1u_2^2u_3^2-2u_1x_2u_2u_3^2+2x_1u_3^4-2u_1x_3u_3^3$
g_2^2	$-u_1^2u_3^2x_3^2+2u_1u_3^3x_1x_3-u_3^4x_1^2$
g_2g_3	$-2x_2x_3u_1^2u_3^2+2x_2u_1u_3^3x_1+2u_2x_3u_1u_3^2x_1-2u_2u_3^3x_1^2$
g_2	$2x_2u_1^2u_3^2-2u_2x_1u_1u_3^2+2x_2u_3^4-2u_2x_3u_3^3$
g_3^2	$-u_1^2u_3^2x_2^2+2u_1u_2u_3^2x_1x_2-u_2^2u_3^2x_1^2$
g_3	$-2x_3u_1^2u_3^2+2x_1u_1u_3^3-2x_3u_2^2u_3^2+2x_2u_2u_3^3$
$-\frac{1}{b^2}$	$u_1^2u_3^2x_2^2+u_1^2u_3^2x_3^2-2u_1u_2u_3^2x_1x_2-2u_1u_3^3x_1x_3+u_2^2u_3^2x_1^2$ $+u_2^2u_3^2x_3^2-2u_2u_3^3x_2x_3+u_3^4x_1^2+u_3^4x_2^2$
1	$u_1^2u_3^2+u_2^2u_3^2+u_3^4$

APPENDIX B

START SYSTEM FOR LOS OBSERVATIONS

The start system used for the homotopy solver was a system with structure equivalent to that of an IOD problem, with parameters sampled randomly in the complex space. The parameters that have been used to build the system are the 8 entries of each $\mathbf{A}_i$ matrix. For five observations, the total number of parameters is 40.

$A_{1,11}$	$-.19554589539818221 - .98069455122016624i$
$A_{1,12}$	$-.99320315995912256 + .11639365552818406i$
$A_{1,21}$	$.84746698926735253 - .53084809701281677i$
$A_{1,22}$	$-.524980096821274 - .85111450342567052i$
$A_{1,31}$	$-.33974371842408813 - .94051805181579262i$
$A_{1,32}$	$-.89716989946776304 - .44168560253760136i$
$A_{1,41}$	$-.70890532572927145 + .70530365031855291i$
$A_{1,42}$	$-.26370047476472958 - .96460461309743706i$
$A_{2,11}$	$-.20422524867817432 + .97892392339871737i$
$A_{2,12}$	$.55012385063274361 - .83508307907956247i$
$A_{2,21}$	$.48701168829251434\,10^{-1} + .99881339406050451i$
$A_{2,22}$	$.67153436779477971 + .74097340901712905i$
$A_{2,31}$	$-.6556966682266403 - .75502442296688865i$
$A_{2,32}$	$-.9906629251051452 + .13633403398314534i$
$A_{2,41}$	$.94618769124965252 + .32361837544807653i$
$A_{2,42}$	$-.92997256157571673 - .36762893617926712i$
$A_{3,11}$	$-.71993815493282887 - .69403822162177353i$
$A_{3,12}$	$.9102476473261466 - .41406427102228338i$
$A_{3,21}$	$.37037792095318434\,10^{-1} - .999313865588136 4i$
$A_{3,22}$	$.85689830118753274 - .51548550069029131i$
$A_{3,31}$	$-.96084848759534092 + .27707432917133623i$
$A_{3,32}$	$.84465300850628211 + .53531420233474702i$
$A_{3,41}$	$.9557472403287276 - .29418907628262025i$
$A_{3,42}$	$-.50996960810970904 + .86019241963901882i$
$A_{4,11}$	$.12465589261909474\,10^{-1} - .99992230152365003i$
$A_{4,12}$	$-.79735359444034148 - .60351242359463264i$
$A_{4,21}$	$-.96223219094239298 - .27223006945266398i$
$A_{4,22}$	$-.95443598913461181 - .29841572117540194i$
$A_{4,31}$	$.39310122113312518 + .919495203872019i$
$A_{4,32}$	$-.97526716110145639 + .22102932944997564i$
$A_{4,41}$	$.91690520139072273 - .39910506343898744i$
$A_{4,42}$	$-.82176111603594681 + .56983214034604535i$
$A_{5,11}$	$-.80802824211988533 - .58914375150437437i$
$A_{5,12}$	$.618733610744305 + .78560086490234649i$
$A_{5,21}$	$-.62005116982349695 - .78456137223324529i$
$A_{5,22}$	$-.19697686571988315 + .9804081366304398i$
$A_{5,31}$	$.73391116358911368 + .67924546664609631i$
$A_{5,32}$	$.17194444870208295 - .98510664730298958i$
$A_{5,41}$	$.62821239391458206 - .77804189355850883i$
$A_{5,42}$	$-.10142870013926006 - .99484281109533079i$

REFERENCES

[1] C. L. Hollenberg and J. A. Christian, "Geometric solutions for problems in velocity-based orbit determination," *The Journal of the Astronautical Sciences*, vol. 67, pp. 188–244, 2019.

[2] J. A. Christian and C. L. Hollenberg, "Initial orbit determination from three velocity vectors," vol. 42, no. 4, 2019.

[3] J. A. Christian, "Analytic initial orbit determination using satellite streaks in digital image," in *AAS/AIAA Astrodynamics Specialist Conference*, 2021.

[4] D. Merrit, K. Garret, and D. Gintaras, "Dark matter: A primer," *Advances in Astronomy*, vol. 2011, 2011.

[5] A. J. Butrica, *The navigators, a history of NASA's deep-space navigation*. CreateSpace Independent Publishing Platform, 2014.

[6] J. Light, "An investigation of the orbit redetermination process following the first midcourse maneuver," in *JPLSPS 37-33:IV*.

[7] J. A. Kennewell and B.-N. Vo, "An overview of space situational awareness," in *Proceedings of the 16th International Conference on Information Fusion*, 2013, pp. 1029–1036.

[8] J. Kepler, *Tabulae Rudolphinae*. 1627.

[9] W. Applebaum, "Keplerian astronomy after Kepler: researches and problems," *History of Science*, vol. 34, no. 4, 1996.

[10] I. Newton, *Philosophiae Naturalis Principia Mathematica*. London, UK: Jussu Societatis Regiae ac Typis Josephi Streater, 1687.

[11] M. Nauenberg, "Newton's graphical method for central force orbits," *American Journal of Physics*, vol. 86, no. 765, 2018.

[12] A. Albouy, "Lambert's theorem: Geometry or dynamics?" *Celestial mechanics and Dynamical Astronomy*, 2019.

[13] L. Eulero, "Theoria motuum planetarum et cometarum," *Euler Archive-All Works*, vol. 66, 1744.

[14] I. Lambert, *Insigniores orbitae cometarum proprietates (1761)* (Kessinger's Legacy Reprints). Kessinger Publishing, LLC, 2010.

[15] J. Lagrange, "Sur le Problème de Kepler," in *Oeuvers, III*, Paris, 1769.

[16] S. Laplace, "Mémoire sur la détermination des orbites des cométes," *Mémoires de l'Academie Royale des Sciences de Paris, Collected Works*, vol. X, pp. 93–146, 1780.

[17] C. Gauss, *Theoria Motus Corporum Coelestium in Sectionibus Conics Solem Ambientium* (Cambridge Library Collection-Mathematics Ser.). Cambridge University Press, 2011.

[18] D. A. Vallado, *Fundamentals of Astrodynamics and Applications* (Space Technology Library). Springer Dordrecht, 2001.

[19] A. C. Long, J. O. Cappellari, C. E. Velez, and A. J. Fuchs, *Goddard Trajectory Determination System (GTDS), Mathematical Theory, Revision 1*. Greenbelt, MD: Goddard Space Flight Center: National Aeronautics and Space Administration, 1989.

[20] P. R. Escobal, *Methods of orbit determination*. New York: John Wiley and Sons, 1965.

[21] J. Gibbs, *On the Determination of Elliptic Orbits from Three Complete Observations*. Hamburg: Frid. Perthes, I. H. Besser, 1889.

[22] T. Duff, M. Mancini, A. Leykin, and J. A. Christian, "Geometric initial orbit determination from bearing measurements," in *AAS/AIAA Astrodynamics Specialist Conference*, Charlotte,NC, 2022.

[23] B. D. Tapley, B. E. Schutz, and G. H. Born, *Statistical Orbit Determination*. Elsevier Academic Press, 2004.

[24] A. Einstein, "On the electrodynamics of moving bodies," *Annalen Der Physik*, pp. 891–921, 1905.

[25] J. V. Field and J. J. Gray, *The Geometrical Work of Girard Desargues*. New York: Springer-Verlag, 1987.

[26] A. of Perga, *Conics, Book I*, Revised. Dana Densmore Edition, 2011.

[27] J. V. Poncelet, *Traité des Propriétés Projectives des Figures*. Paris: Gauthier Villars, 1865.

[28] J. G. Semple and G. T. Kneebone, *Algebraic Projective Geometry*. New York: Oxford University Press, 1952.

[29] R. Hartley and A. Zisserman, *Multiple View Geometry in computer vision*, 2nd ed. Cambridge University Press, 2003.

[30] J. Harris, *Algebraic Geometry, a first course* (Graduate Texts in Mathematics). New York: Springer Science+Business Media, LCC, 1992.

[31] N. J. Wilderberger, *Macaulay2 software*, https://njwildberger.com/.

[32] R. Bate, D. Mueller, J. White, and W. Saylor, *Fundamentals of Astrodynamics*, 2nd ed. Mineola, New York: Dover Publications Inc., 2020.

[33] T. Duff, C. Hill, A. Jensen, K. Lee, A. Leykin, and J. Sommars, "Solving polynomial systems via homotopy continuation and monodromy," *IMA Journal of Numerical Analysis*, vol. 39, Sep. 2016.

[34] T. Chen and T.-Y. Li, "Homotopy continuation method for solving systems of nonlinear and polynomial equations," *Communications in Information and Systems*, vol. 15, pp. 119–307, Jan. 2015.

[35] S. Gao, "Counting zeros over finite fields with gröbner bases," Jan. 2009.

[36] C. L. Parkinson, "Aqua: An earth-observing satellite mission to examine water and other climate variables," *IEEE Transactions on Geoscience and Remote Sensing*, vol. 41, no. 2, pp. 173–183, 2003.

[37] A. Leykin and R. Krone, *Macaulay2 software*, http://www2.macaulay2.com/Macaulay2/.

[38] M. D. Shuster and S. D. Oh, "Three-axis attitude determination from vector observations," *Journal of Guidance and Control*, vol. 4, no. 1, pp. 70–77, 1981.

[39] M. D. Shuster, "Maximum likelihood estimation of spacecraft attitude," *The Journal of the Astronautical Sciences*, vol. 37, no. 1, pp. 79–88, 1989.

[40] S. A. Fuselier *et al.*, "Magnetospheric multiscale science mission profile and operations," *Space Science Reviews*, pp. 77–103, 2014.

[41] A. Petit, T. Antoun, J. Vaubaillon, R. Lucken, F. Delefie, and D. Giolito, "Streak detection challenges for telescope observations of satellites," in *Proc. 8th European Conderence on Space Debris*, Darmstadt, Germany: ESA Space Debris Office, 2021.

[42] R. M. L. Baker and N. H. Jaboby, "Preliminary orbit-determination method having no-coplanar singularity," *Celestial Mechanics*, vol. 15, pp. 137–160, 1977.